Global Biogeochemical Cycles

RESEARCH ARTICLE
10.1029/2022GB007333

Special Section:
REgional Carbon Cycle Assessment and Processes - 2

Significant Seasonal N_2O Dynamics Revealed by Multi-Year Observations in the Northern South China Sea

Xianhui S. Wan[1,2], Hua Lin[1,3], Bess B. Ward[2], Shuh-Ji Kao[1], and Minhan Dai[1]

[1]State Key Laboratory of Marine Environmental Sciences, Xiamen University, Xiamen, China, [2]Department of Geosciences, Princeton University, Princeton, NJ, USA, [3]Key Laboratory of Marine Ecosystem Dynamics, Second Institute of Oceanography, Ministry of Natural Resources, Hangzhou, China

Abstract The coastal ocean and marginal sea play a disproportionally important role in the release of nitrous oxide (N_2O) into the atmosphere. The spatial and temporal distribution of N_2O in these important source regions remains highly uncertain due to the scarcity of N_2O measurements. Here we present a large data set of N_2O concentrations and fluxes obtained from 10 cruises covering four seasons in the Northern South China Sea (NSCS). The study area is overall a net source of atmospheric N_2O with an annual flux of $1.9 \pm 1.2 \times 10^8$, $0.8 \pm 0.5 \times 10^8$ and $1.2 \pm 0.7 \times 10^8$ mol N_2O yr^{-1} in the shelf, slope and basin regions, respectively. In terms of global warming potentials, the N_2O emissions offset 27.8% of the CO_2 sink on the shelf, and are equivalent to 3.5 and 0.2-fold of the CO_2 emission in the slope and basin of the NSCS. On the seasonal time scale, N_2O flux was significantly higher in autumn and winter than in the warm seasons. The spatial variability was contrastingly less pronounced. The seasonality of N_2O distribution in the shelf region was modulated by the riverine discharge, while intrusion of the Kuroshio Current exerted profound control on N_2O distribution in the open waters of the NSCS. The variable relationships between N_2O excess, apparent oxygen utilization, and nitrate in the shelf, NSCS basin and the Luzon Strait indicated a regional difference in N_2O cycling pathways along with the impact of water mass mixing. Our study establishes a robust baseline to understand N_2O distribution and flux in the NSCS.

Xianhui S. Wan and Hua Lin contributed equally to this work.

Key Points:

- N_2O dynamics demonstrate significant seasonal, but much less pronounced spatial variations in the Northern South China Sea
- Annual N_2O emmision offset 28% of the CO_2 sink on the shelf, and are equivalent to 249% and 23% of the CO_2 emission in the slope and basin
- Riverine discharge and Kuroshio Current intrusions are the main drivers of N_2O dynamics in the Northern South China Sea

Supporting Information:

Supporting Information may be found in the online version of this article.

Correspondence to:

M. Dai,
mdai@xmu.edu.cn

Citation:

Wan, X. S., Lin, H., Ward, B. B., Kao, S.-J., & Dai, M. (2022). Significant seasonal N_2O dynamics revealed by multi-year observations in the Northern South China Sea. *Global Biogeochemical Cycles*, *36*, e2022GB007333. https://doi.org/10.1029/2022GB007333

Received 28 JAN 2022
Accepted 3 OCT 2022

Author Contributions:

Conceptualization: Xianhui S. Wan, Hua Lin, Minhan Dai
Data curation: Xianhui S. Wan, Hua Lin, Minhan Dai
Formal analysis: Xianhui S. Wan, Hua Lin, Bess B. Ward, Shuh-Ji Kao, Minhan Dai
Funding acquisition: Minhan Dai
Investigation: Xianhui S. Wan, Hua Lin, Minhan Dai
Methodology: Xianhui S. Wan, Hua Lin, Minhan Dai

1. Introduction

Nitrous oxide (N_2O) is a trace gas that causes global concern as a greenhouse gas (GHG) with ozone depletion capacity (Canadell et al., 2021; Ravishankara et al., 2009). The concentration of N_2O in the atmosphere has been increasing at an accelerating pace due largely to anthropogenic perturbation since the onset of the industrial era, contributing substantially to the global GHG budget (Battaglia and Joos, 2018; Prinn et al., 2018; Tian et al., 2020). Accurately estimating the N_2O fluxes from various sources is thus critical for understanding the role of N_2O in the climate system.

The ocean is an important source of atmospheric N_2O, accounting for over 20% of total annual N_2O emissions to the atmosphere (Canadell et al., 2021; Tian et al., 2020). Since the first observation of N_2O distribution in the marine environment in the 1960s (Craig and Gordon, 1963), N_2O concentration measurements have been conducted in nearly all ocean basins and in many coastal and marginal seas (Bange et al., 2019; Yang et al., 2020). N_2O concentrations vary over four orders of magnitude in different marine systems, ranging from <1 nmol L^{-1} in the anoxic core of the Black Sea (Westley et al., 2006) to >1000 nmol L^{-1} in the near surface of oxygen minimum zones (Arévalo-Martínez et al., 2015) and some hyper-eutrophic coastal areas (Barnes and Upstill-Goddard, 2011). In the surface water, the highest levels of N_2O saturation are generally observed in nearshore and tropical upwelling regions (Yang et al., 2020), while in the vast subtropical oligotrophic oceans, surface N_2O concentration is generally only slightly oversaturated with respect to air equilibrium (Wilson et al., 2017; Yang et al., 2020). These observations establish an important baseline for general spatial distribution of N_2O concentrations in the global ocean.

The air-sea N_2O fluxes are highly variable in both space and time (Bange et al., 2019; Canadell et al., 2021; Wilson et al., 2020; Yang et al., 2020), and they are challenging to constrain because both excess N_2O (ΔN_2O) and the transfer velocity (k) are regulated by multiple environmental factors such as temperature, salinity, N_2O concentration, wind speed, and boundary layer dynamics (Wanninkhof et al., 2009). Consequently, quantitative estimates of N_2O fluxes are highly uncertain and inconsistent among studies (Battaglia and Joos, 2018; Buitenhuis et al., 2018; Canadell et al., 2021; Freing et al., 2012; Ji et al., 2018; Manizza et al., 2012; Nevison

Resources: Shuh-Ji Kao, Minhan Dai
Validation: Xianhui S. Wan, Hua Lin, Bess B. Ward, Shuh-Ji Kao, Minhan Dai
Visualization: Xianhui S. Wan, Bess B. Ward, Shuh-Ji Kao
Writing – original draft: Xianhui S. Wan, Hua Lin, Minhan Dai
Writing – review & editing: Xianhui S. Wan, Hua Lin, Bess B. Ward, Shuh-Ji Kao, Minhan Dai

et al., 1995; Yang et al., 2020). Among others, these inconsistencies suggest that N_2O measurements are still insufficient to resolve the variability of marine N_2O at multiple spatial and temporal scales, and our understanding to N_2O production and consumption across different marine environments is to be improved (Bange et al., 2019). Though a recent meta-analysis of the global air-sea N_2O flux was able to resolve a seasonal cycle with markedly reduced uncertainty (Yang et al., 2020), the volume of the datasets (~158,000 N_2O observations) used remains much smaller than that available for sea surface CO_2 (>14.7 million values) (Bakker et al., 2016). A handful of studies point to the significant seasonality of air-sea N_2O flux (Capelle et al., 2018; Farías et al., 2015; Nevison et al., 2005; Wilson et al., 2017; Yang et al., 2020); however, observations covering the seasonal cycle of marine N_2O distribution and emission remain sparse in the global ocean.

N_2O is an intermediate or a byproduct of multiple processes in the nitrogen cycle, among which ammonia oxidation, nitrifier-denitrification, and denitrification are considered the main processes responsible for N_2O production (Stein and Yung, 2003; Wrage et al., 2001). The relative importance of these pathways, however, varies across time and space in marine environments. Changes in environmental conditions such as temperature, dissolved oxygen (DO), pH, and nutrient input may significantly modulate N_2O production rate and the underlying process, resulting in large uncertainty in predicting the sources and flux of marine N_2O in a changing ocean (Battaglia and Joos, 2018; Breider et al., 2019; Ji et al., 2018; Landolfi et al., 2017; Rees et al., 2016; Suntharalingam et al., 2012, 2019). Correlation analysis between N_2O and specific environmental parameters provides valuable information about the source and environmental control on N_2O production and distribution. Among these, correlation analysis between excess N_2O (ΔN_2O) and apparent oxygen utilization (AOU) or nitrate (NO_3^-) is a widely used approach to evaluate the source process and the strength of N_2O production in the oxygenated ocean. The strong correlation between ΔN_2O and AOU is generally considered as evidence of N_2O production by nitrification (Butler et al., 1989; Carrasco et al., 2017; de la Paz et al., 2017; Nevison et al., 1995, 2003; Tseng et al., 2016; Yoshinari, 1976). The coefficient between ΔN_2O and AOU varies among different oceanic provinces and depths, which might be caused by complex physical-biological processes, including the variable N_2O yield during nitrification (Nevison et al., 2003), N_2O consumption in low oxygen environments (De Wilde and Helder, 1997), the increasing atmospheric N_2O concentration (Freing et al., 2009), the deviation of O_2 equilibration with air when water masses are formed (de la Paz et al., 2017), O_2 production by photosynthesis (Capelle et al., 2018), and water mass mixing (Carrasco et al., 2017; Martinez-Rey et al., 2015). Moreover, the importance of these factors in determining the observed ΔN_2O and AOU relationship appears to vary among depths and regions (de la Paz et al., 2017; Martinez-Rey et al., 2015; Nevison et al., 2003). Therefore, the underlying reason for the variation in the ΔN_2O and AOU relationship is complicated and needs to be addressed before being used for extrapolation or model parameterization.

Ocean margins are significant global N_2O sources to the atmosphere, playing a disproportionate role in contributing to the atmospheric N_2O reservoir (Arévalo-Martínez et al., 2015; Bange, 2006; Kock et al., 2016; Murray et al., 2015; Yang et al., 2020). The air-sea N_2O flux, however, remains poorly constrained due largely to the coarse spatial-temporal resolution of N_2O measurements in the ocean margins. Thus, there is an urgent need to expand N_2O observations in these intensive source regions to better constrain the global N_2O budget (Wilson et al., 2020). In this study, we present seven consecutive years of observations of N_2O distribution extending from shelf into basin of the Northern South China Sea (NSCS). The primary motivations of our study are to (a) characterize the spatial distribution and seasonal variation of N_2O in the NSCS; (b) estimate the flux of N_2O from the investigated area to the atmosphere with particular attention to its seasonal variability; and (c) identify the potential sources of N_2O and their environmental constraints. The results provide a baseline for long-term N_2O measurement which will help further constraining uncertainties of the air-sea N_2O flux in the NSCS.

2. Materials and Methods

2.1. Study Area

The SCS is the largest marginal seas of the North Pacific Ocean, with an area of 3.5×10^6 km^2 and an average depth of 1,350 m (Chen et al., 2001; Hu et al., 2000). The SCS basin is a typical oligotrophic system featuring preeminent stratification. The SCS is semi-enclosed and exchanges with the adjacent western Philippine Sea (WPS) through the Luzon Strait, the only gateway for intermediate and deep-water exchanges (Figure 1) (Dai et al., 2013 and references therein). By contrast, the western and northern boundaries of the SCS have extensive shelf systems that receive a large amount of terrestrial nutrients primarily through riverine export, which

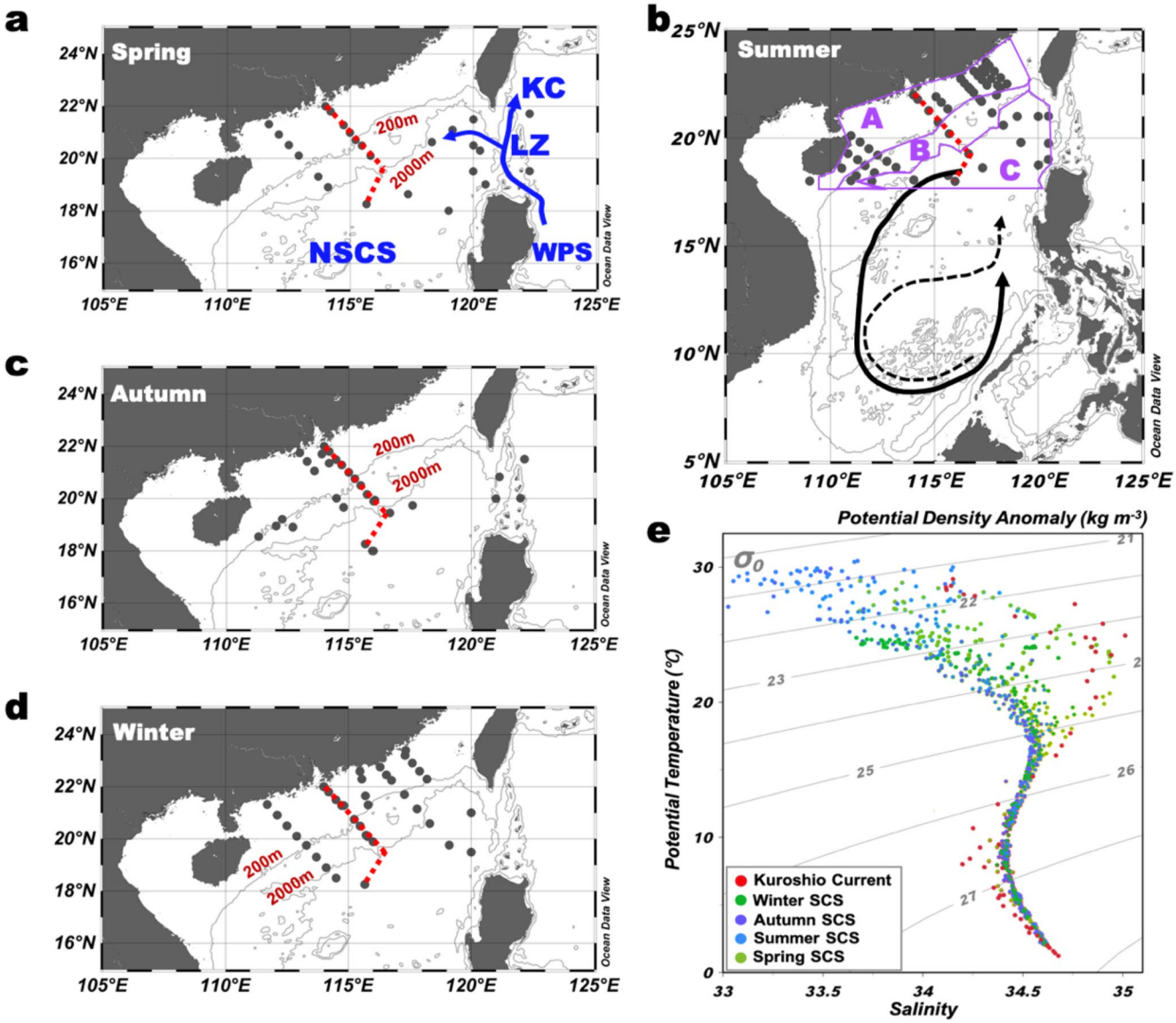

Figure 1. Sampling stations and T-S diagram of the sampling depths. (a)–(d) Sampling stations in spring, summer, autumn, winter, respectively. (e) T–S diagram at the stations with bottom depth >200 m. The red dashed lines in (a)–(d) denote transect A for repeated investigation in all four seasons. The isobaths of 200 and 2000 m shown in gray lines define the shelf (0–200 m), slope (200–2000 m), and basin (>2,000 m). The NSCS, WPS, and LZ in panel (a) denote the Northern South China Sea, Western Philippine Sea and Luzon Strait, respectively. The schematic pathway of Kuroshio Current (KC) and its intrusion through the Luzon Strait into the Northern SCS is also shown in panel (a) (blue solid lines). The black lines in panel (b) show the basin wide surface circulation pattern in winter (solid line) and summer (dashed line). The boundaries of shelf (a), slope (b), and basin (c) of the NSCS used for our zonal air-sea N_2O flux estimation are shown in purple in panel (b).

in turn sustains higher biological activities than the basin (Chen et al., 2001; Lu et al., 2020). The seasonal climatic variation and surface circulation of the SCS are mainly determined by the Asian monsoon: the warm and wet southwest monsoon season prevails from May to October, shaping an anticyclonic circulation pattern at basin scale. The northeast monsoon, which is characterized by cold and high wind speed, prevails from November through April, resulting in a cyclonic surface circulation structure. Meanwhile, the northeastern prevailing wind in wintertime reduces the northward momentum of the Kuroshio Current (KC), a northward branch of the ultra-oligotrophic North Equatorial Current, which allows a higher proportion of KC water intrusion into the SCS (Wong et al., 2007; Zhu et al., 2019). Thus, the surface water in the SCS basin is comprised of a set of water masses, including river plume, the SCS surface water and the KC surface water, whose relative contributions vary spatially according to variable seasonal forcing.

Table 1
Summary of Cruises to the Northern South China Sea (NSCS) and Sampling Information

Cruise	Study area	Season	Stations	Samples
July 2007	NSCS	Summer	5	67
July 2008	NSCS	Summer	25	134
September 2008	Luzon Strait	Summer	3	35
January 2009	NSCS	Winter	16	96
July 2009	NSCS	Summer	32	304
January 2010	NSCS	Winter	26	222
November 2010	NSCS	Autumn	21	169
May 2011	NSCS and Luzon	Spring	21	204
September–October 2012	NSCS	Autumn	7	111
April 2013	NSCS and Luzon	Spring	5	117

2.2. Cruises and Sample Collections

Samples were collected during 10 cruises covering four seasons in seven consecutive years. A total of 161 stations and over 1,450 depths were sampled for N_2O, DO, and nutrients (Table 1). The shelf (0–200 m), slope (200–2,000 m), and basin (>2,000 m) of NSCS were investigated at all seasons, and the Luzon Strait was sampled in spring and autumn (Figures 1a–1d).

Temperature, salinity and depth were measured using a Seabird SBE 911 CTD sensor. Discrete seawater samples were collected using 12-L Niskin bottles mounted on the CTD rosette. Duplicate 150 ml high-density polyethylene Nalgene bottles were used for nutrient collection. The bottles and equipment were acid washed and rinsed with seawater three times prior to sample collection. The nutrient samples were stored at −20°C until analysis. Samples for N_2O concentration measurement were subsampled directly from the Niskin bottles into acid-washed, precombusted (450°C for 4 hr) 120 mL serum bottles using Tygon tubing. Each serum bottle was filled to the top and overfilled two to three volumes to minimize the introduction of bubbles. The bottle was then sealed with a 20 mm butyl stopper and aluminum crimp seal (Wheaton, USA), followed by injection of 0.1 mL saturated $HgCl_2$. Samples were stored at 4°C for later laboratory measurement. Samples for DO concentration measurement were collected into ground glass stoppered bottles and overfilled two to three volumes, and stored briefly until analyses onboard.

2.3. Sample Analysis

N_2O concentration was analyzed using gas chromatography (Hewlett-Packard Model 6890) connected to a purge and trap system (Tekmar Velocity XPT) (Lin et al., 2016). Briefly, 10 mL of sample was transferred into a glass vessel where the sample was purged for 10 min using purified N_2 (>99.999%). N_2O from the sample was trapped on a 5 Å molecular sieve at room temperature and subsequently desorbed at 250°C. A micro-electron capture detector (μECD) was used to measure N_2O concentration. Calibration of N_2O concentrations was calculated from the peak areas with standard gases of 1.0–5.0 ppmv N_2O/N_2 (Research Institute of China National Standard Materials). The precision of this method was estimated to be better than ±3% (Lin et al., 2016).

DO concentration was measured onboard using the Winkler method, and the precision was <2 μmol kg^{-1}. Nitrate plus nitrite (NO_X^-) was determined according to classical colorimetric methods with an AA3 nutrient analyzer. The detection limit for NO_X^- was 0.03 μmol L^{-1}, and the analytical precision was better than ±1% (Han et al., 2012).

2.4. Saturation and Air-Sea Flux Calculation

AOU represents the consumption of DO in a water parcel since its last equilibration with the atmosphere. It can be calculated as the difference between the measured DO concentration and the calculated oxygen solubility at the sampling salinity and temperature. However, due to the vigorous air-sea exchange and the biological O_2

production, AOU cannot be reliably computed in the euphotic ocean (Capelle et al., 2018; de la Paz et al., 2017; Nevison et al., 1995). Thus, AOU in the euphotic zone (i.e., <100 m) was excluded from our study.

Surface N_2O saturation was calculated using Equation 1.

$$R = \frac{C_{obs}}{C_{eq}} \times 100 \quad (1)$$

where R (%) is the saturation of surface N_2O; C_{obs} represents N_2O concentration at 5 m depth; C_{eq} is the expected equilibrium concentration, which is computed using Henry's Law and the solubility as a function of temperature and salinity (Weiss and Price, 1980). The atmospheric mixing ratios of N_2O were obtained from the NOAA/ESRL program sampling station at Mauna Loa in the sampling month from NOAA/ESRL program (https://gml.noaa.gov/ccgg/trends_n2o/) (Dlugokencky, 2022).

The ΔN_2O represents the net accumulation of N_2O during the aging of a water parcel. It was calculated as the difference between the calculated N_2O equilibrium concentration and the measured concentration of N_2O. Taking the distinct age (thereby the different atmospheric N_2O concentration) of the water mass at different depths, we used the "initial atmospheric mole fraction" to calculate the ΔN_2O at different depths (Freing et al., 2009; Nevison et al., 2003; Walter et al., 2006). Specifically, the water column was vertically divided into three layers based on the source of water masses: the upper layer (σ_θ < 26.4 kg m^{-3}, typically ~300 m in the NSCS), the intermediate layer (σ_θ: 26.4–27.6 kg m^{-3}, from the base of upper layer to 1,500 m), and the deep layer (σ_θ > 27.6 kg m^{-3}, deeper than 1,500 m) (Zhu et al., 2019). For the upper layer, strong vertical transport and mixing lead to short residence time (<2 years) (Liu and Gan, 2017). Thus, the contemporary atmospheric N_2O concentration during the sampling period was used in the upper layer (0–300 m). For the intermediate (300–1500 m) and deep layer (>1500 m), the air N_2O concentration used for N_2O equilibrium calculation is derived by the aging of the water mass. The age of the intermediate water is estimated to be 500–900 years in the western North Pacific Ocean (England, 1995), and the age of deep water is 1,200–1,500 years (Gebbie and Huybers, 2012). Therefore, we use the air N_2O concentration of 270 and 260 ppb for calculating the N_2O equilibrium of the intermediate and deep layers, respectively (MacFarling Meure et al., 2006). It should be noted that the age of the water mass at different depths in the water column could vary and remains uncertain due to active vertical and horizontal water exchange in the study area (Liu and Gan, 2017; Zhu et al., 2019). Thus, using a fixed air N_2O concentration for the intermediate and deep layers might lead to uncertainties in calculating the ΔN_2O. However, given that the variation of air N_2O concentration in the intermediate and deep layers is relatively small (i.e., range from ~260 to ~270 ppb), the difference of the ΔN_2O estimated using these air N_2O concentrations was 2.9 ± 0.8% (range 1.6%–5.9%) in our study (Figure S1 in Supporting Information S1).

Air-sea N_2O flux was computed using Equations 2 and 3.

$$F = k \times \left(C_{obs} - C_{eq}\right) \quad (2)$$

$$k = 0.251 \times u^2 \times \left(\frac{S_c}{660}\right)^{-0.5} \quad (3)$$

where F (μmol N_2O m^{-2} d^{-1}) is air-sea flux of N_2O, k (cm h^{-1}) is the gas transfer velocity following Wanninkhof (2014), and k is a function of wind speed and temperature through its Schmidt number dependency; u is monthly mean wind speed at 10 m above sea surface during the cruise, using monthly averaged QuikScat wind speeds (ftp://ftp.ssmi.com/qscat/). S_c is the Schmidt number calculated from temperature (Wanninkhof, 2014).

The regional air-sea N_2O flux was derived by integrating N_2O fluxes of all four seasons in the NSCS. To better characterize and compare the spatial-seasonal variation of the air-sea flux, the study area was subdivided into three domains (the shelf, slope and basin) based on the physical-biological characteristics as described previously (Li et al., 2020; Zhai et al., 2013). The extent of the NCSC was defined as 18–24°N, 109.5–20.5°E. The boundary of each domain was based on the 200 and 2,000 m isobath (Figure 1b). The areas of shelf, slope and basin are 0.25×10^6 km^2, 0.12×10^6 km^2, and 0.21×10^6 km^2, respectively. The seasonal air-sea flux of each domain was derived as the area multiplied by the area-weighted average flux of the investigated stations in each season. The annual air-sea flux of each domain was then calculated as the sum of four seasons.

2.5. Vertical N_2O Flux Across the Base of Euphotic Zone

Vertical N_2O flux across a certain depth can be estimated using a one-dimensional vertical diffusion-advection model using Equation 4.

$$F = K_V \frac{\partial c}{\partial z} + \omega c \tag{4}$$

where K_V is the diapycnal diffusivity, ω is the diapycnal velocity in the vertical direction, $\partial c/\partial z$ is the concentration gradient, c is the N_2O concentration in the layer. K_V and ω in the study area were adapted from observations at the South East Asian Time-series Study (SEATs) station located in the NSCS basin (Du et al., 2017), where K_V and ω were 0.05 $cm^2\ s^{-1}$ and 4×10^{-8} m s^{-1} at the 100 m, respectively. Notably, the application of one-dimension model is based on the assumption that lateral transport is insignificant. However, both the shelf of the NSCS and the Luzon Strait areas are characterized by active lateral processes (Zhu et al., 2019), thus, the one-dimensional model used here is restricted to the NSCS basin area.

3. Results

3.1. Hydrography

The T–S diagram showed distinct physical properties between the NSCS and the Luzon Strait (Figure 1e). In the upper layer (i.e., from the surface to the salinity maximum), the Luzon Strait showed higher salinity and temperature than the NSCS interior, demonstrating typical properties of the KC surface water. In the NSCS, the T–S data were more scattered due to the mixing of KC water, the NSCS tropical water and coastal current (Wu et al., 2021). By contrast, in the intermediate layer, salinity decreased with depth from the salinity maximum to the salinity minimum layer at both SCS and the Luzon Strait stations, while the minimum value in the western Pacific was lower than the NSCS at the corresponding layer. The T–S relationship in the deep layer was near homogenous in the study area as the deep water of NSCS essentially originated from the western Pacific deep water (Chen, Shaih, et al., 2006; Chen, Hou, et al., 2006). Overall, the vertical gradients of temperature and salinity were less pronounced in the NSCS than the Luzon Strait stations owing to more intense vertical mixing and upwelling at the basin scale in the NSCS (Wong et al., 2007; Zhu et al., 2019).

In the surface water, a clear seasonality of temperature was observed at the NSCS stations (Figure 2; Figure S2a and Table S1 in Supporting Information S1); the highest temperature (average: 28.3 ± 1.7°C) was measured in summer, followed by spring (27.5 ± 1.1°C), and the temperature in autumn (26.1 ± 2.2°C) and winter (22.0 ± 2.5°C) was significantly lower than in the warm seasons ($p < 0.01$). By contrast, the salinity in summer (32.6 ± 1.9) and autumn (33.3 ± 1.0) was lower than in spring (33.9 ± 0.5) ($p < 0.01$), and winter (33.8 ± 0.6) ($p < 0.05$), due to the high riverine discharge and more precipitation in the southwest monsoon (warm) season (Figure 2; Figure S2b in Supporting Information S1) (Cao et al., 2020). Accordingly, the surface density anomaly in spring (21.6 ± 0.4 kg m^{-3}) and summer (21.3 ± 0.8 kg m^{-3}) was significantly lower than in autumn (22.0 ± 0.8 kg m^{-3}) and winter (23.3 ± 0.3 kg m^{-3}) ($p < 0.01$) (Figures 2c, 2f, 2i, and 2l; Figure S2c in Supporting Information S1). In spring and winter, the temperature and salinity of the upper layer in the NSCS were closer to those of the western Pacific, suggesting a higher proportion of KC intrusion into the upper NSCS in these seasons. No significant seasonality was found in the intermediate and deep waters.

3.2. Surface Water N_2O Distribution and Air-Sea N_2O Flux

Surface water NO_x^- concentration decreased from the shelf to the slope and basin in all seasons. Seasonally, the area weighted average surface NO_X^- concentration was highest in autumn (2.4 ± 2.9 μmol L^{-1}), followed by winter (1.0 ± 1.3 μmol L^{-1}) and summer (0.5 ± 1.2 μmol L^{-1}), and was lowest in spring (0.2 ± 0.4 μmol L^{-1}) (Figures 3a, 3d, 3g, and 3j; Figure S2d and Table S1 in Supporting Information S1).

Similarly, the highest surface N_2O concentration was generally observed in the coast and shelf regions (7.3 ± 1.0 nmol L^{-1}) and decreased toward the slope (7.0 ± 0.8 nmol L^{-1}) and basin stations (6.7 ± 0.7 nmol L^{-1}) although the concentration was significantly different only between shelf and basin ($p < 0.01$) (Figures 3b, 3e, and 3h; Table S2 in Supporting Information S1). These values were slightly lower than the values reported by Zhang et al. (2019) in June 2015 but consistent with the observations of Tseng et al. (2016) in summer of 2003

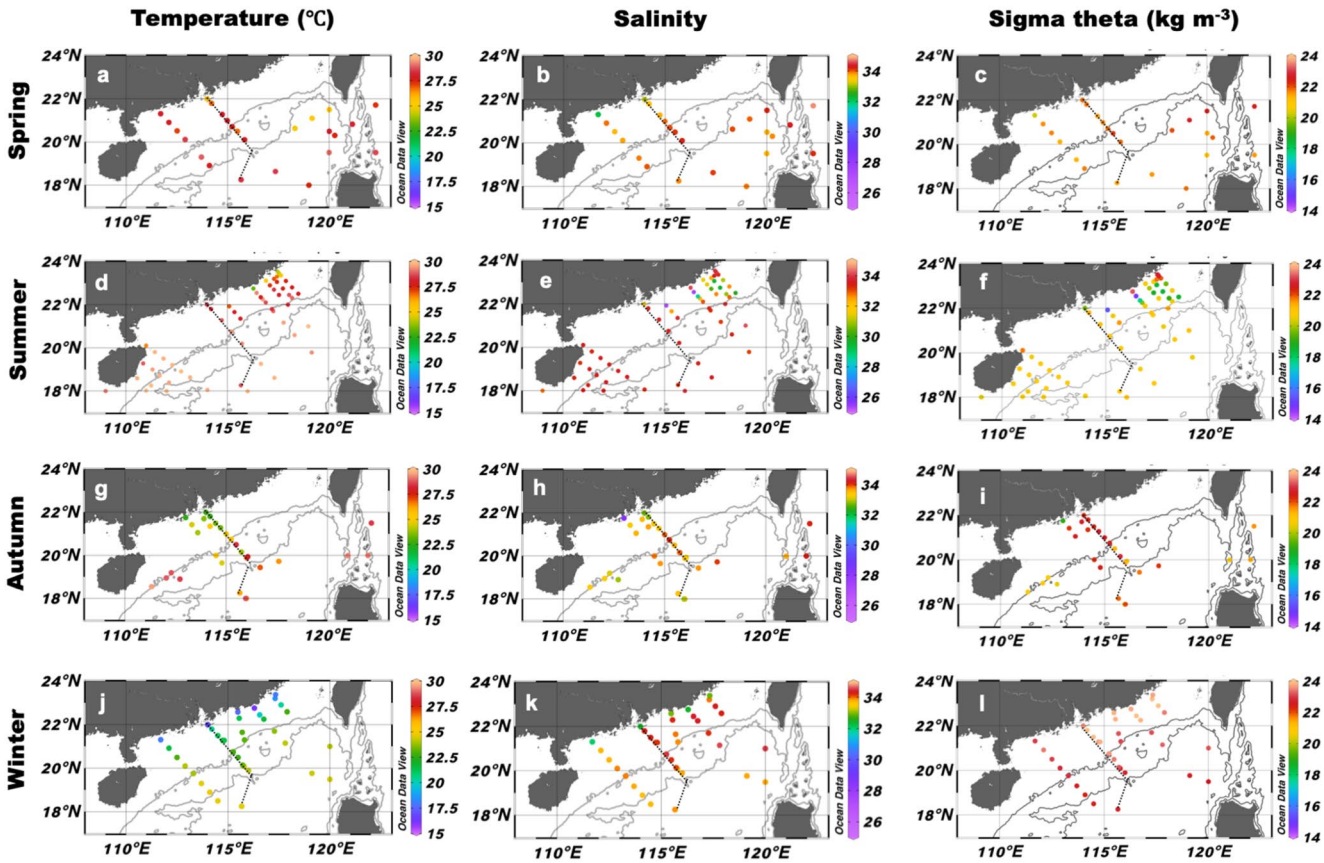

Figure 2. Surface distributions of temperature, salinity and potential density anomaly (sigma theta) at the study area in different seasons. (a)–(c) spring; (d)–(f) summer; (g)–(i) autumn; (j)–(l) winter. The black dashed lines denote transect A.

and 2004 in the study area. However, there was no significant correlation between NO_X^- and N_2O, suggesting different mechanisms for regulating surface NO_X^- and N_2O distribution in the NSCS. Seasonally, the area weighted average N_2O concentration was lower in spring (6.6 ± 0.2 nmol L^{-1}) and summer (6.6 ± 0.5 nmol L^{-1}) than in autumn (7.1 ± 0.3 nmol L^{-1}) and winter (7.8 ± 0.4 nmol L^{-1}) (Figure S2e in Supporting Information S1).

By contrast, surface N_2O saturation did not show a clear spatial pattern as for NO_X^- and N_2O concentration. The saturation ranged from 86.9% to 130.1% (average 108.1 ± 11.6%), 95.9%–139.8% (108.9 ± 10.8%), and 94.9%–117.2% (105.3 ± 7.1%) at the coast, slope, and basin stations, respectively (Figures 3c, 3f, and 3i, 3l). Saturation was higher in summer and autumn, followed by winter and was significantly lower in spring than in summer and autumn ($p < 0.05$) (Figure S2f in Supporting Information S1).

Area weighted average seasonal ΔN_2O (spring 0.3 ± 0.2 nmol L^{-1}, summer 0.5 ± 0.5 nmol L^{-1}, autumn 0.5 ± 0.3 nmol L^{-1} and winter 0.6 ± 0.3 nmol L^{-1}) did not vary significantly (Figure S3a in Supporting Information S1). On the other hand, the wind speed was significantly higher in autumn (9.3 ± 4.2 m s^{-1}) and winter (9.5 ± 1.5 m s^{-1}) than in spring (4.5 ± 0.1 m s^{-1}) and summer (5.6 ± 0.2 m s^{-1}) ($p < 0.01$) (Figure S3b in Supporting Information S1). Accordingly, a strong seasonality of air-sea N_2O flux was observed. The N_2O flux ranged from −0.5 to 1.7 μmol m^{-2} d^{-1}, −0.9 to 9.4 μmol m^{-2} d^{-1}, −2.3 to 8.9 μmol m^{-2} d^{-1}, and −3.8 to 7.5 μmol m^{-2} d^{-1} in spring, summer, autumn, and winter, respectively (Figures 4a–4d). Area weighted N_2O flux was significantly lower in spring (0.4 ± 0.3 μmol m^{-2} d^{-1}) and summer (0.9 ± 1.0 μmol m^{-2} d^{-1}) than in autumn (3.2 ± 1.8 μmol m^{-2} d^{-1}) and winter (2.9 ± 1.9 μmol m^{-2} d^{-1}) at all the investigated regions. The highest N_2O fluxes in shelf and slope regions were observed in autumn, while the flux in the basin was highest in winter (Figures S4a–S4c in Supporting Information S1). By contrast, the average N_2O fluxes in the shelf, slope and basin were not significantly different among seasons (with the exception of autumn, when the flux on the shelf was significantly higher than in basin) (Figures S4d–S4g in Supporting Information S1).

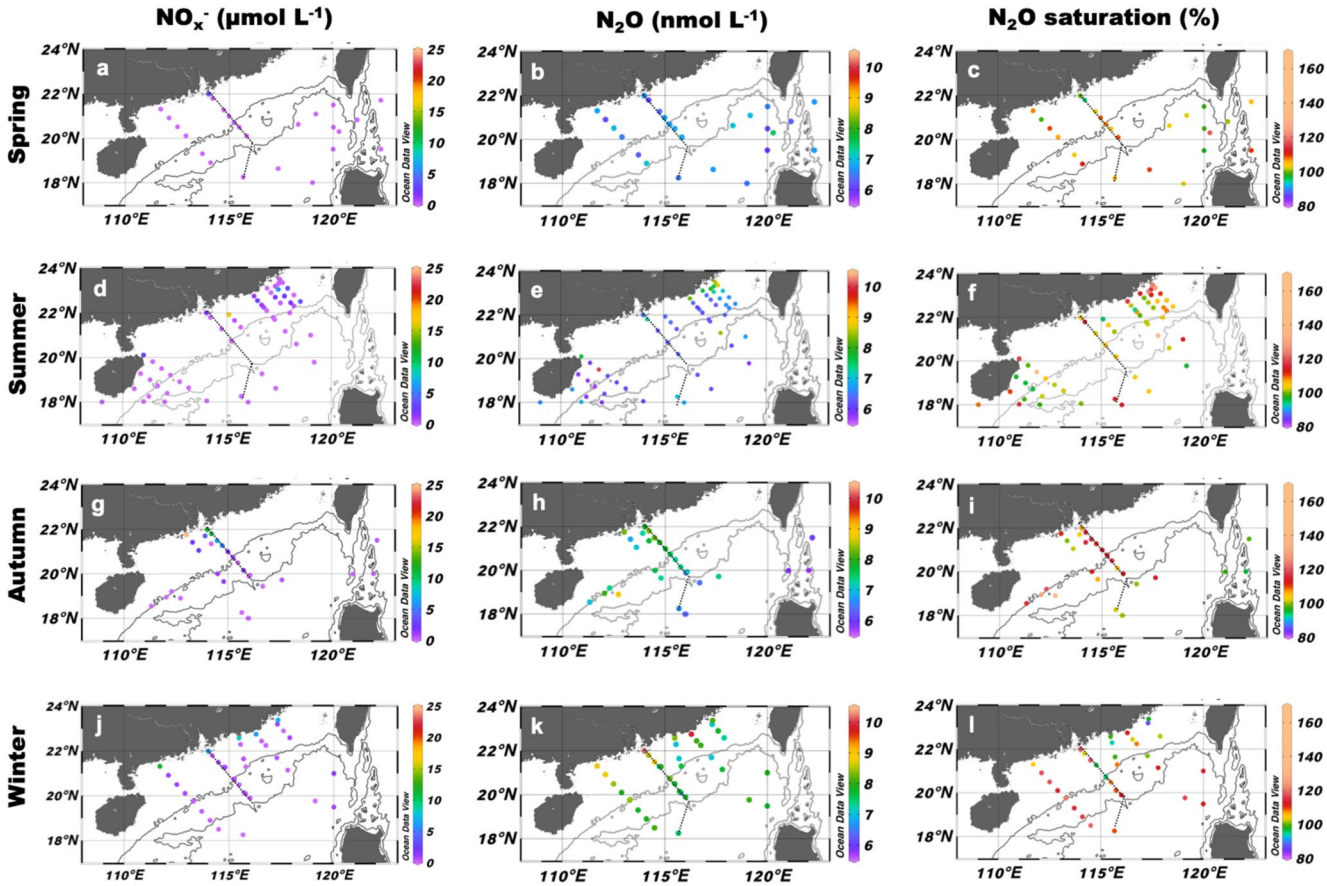

Figure 3. Surface distribution of NO_X^-, N_2O and N_2O saturation at the study area in different seasons. (a)–(c) spring; (d)–(f) summer; (g)–(i) autumn; (j)–(l) winter. The black dashed lines denote transect A.

3.3. N_2O Distribution in the Euphotic Zone

The vertical distribution of N_2O concentrations in the euphotic zone was similar at all stations and in all seasons. N_2O in surface water was nearly equilibrated with the atmosphere and concentration increased toward the base of the euphotic zone. Similar to the surface water, N_2O and NO_X^- concentrations in the upper mixed layer were higher on the shelf than the open waters (Figure 5). To better explore the seasonality of N_2O distribution, a transect extending from the coast to the basin of the NSCS (Transect A) was repeated during all four seasons. Here, we focused on the upper 150 m because the seasonal variability in N_2O was more pronounced in this depth range.

Low surface salinity (i.e., <33) was observed at the shelf stations in all seasons, suggesting the direct influence of riverine discharge (Figures 6a–6d). The salinity of the upper 100 m was highest in spring, followed by winter, indicating stronger intrusion of the KC into the NSCS. The lower salinity in summer and autumn was likely caused by the reduced influence from the KC and higher riverine discharge and precipitation. The greater influence of the KC intrusion into the NSCS in the winter and spring was also evidenced by the more similar T–S structure between the NSCS and the KC in these seasons (Figure 1e). Such a prominent seasonal pattern has been extensively observed by a large body of studies using T–S structure and numerical models, emphasizing a key role of the KC intrusion in determining the physical and biological properties of the NSCS (Du et al., 2013; Gan et al., 2016; Zhu et al., 2019 and references therein). Salinity increased with depth at all stations except at A4 located at the shelf break, which was nearly isohaline except in summer.

In the upper mixed layer, average N_2O and NO_X^- concentrations were elevated in autumn and winter compared to spring and summer (Figures 6e–6h, 6m–6p). The DO had an opposite pattern along the transect, that is, DO was higher at the slope and basin stations, but the seasonality was consistent with that observed for N_2O and NO_X^-, with higher DO concentrations in autumn and winter (Figures 6i–6l).

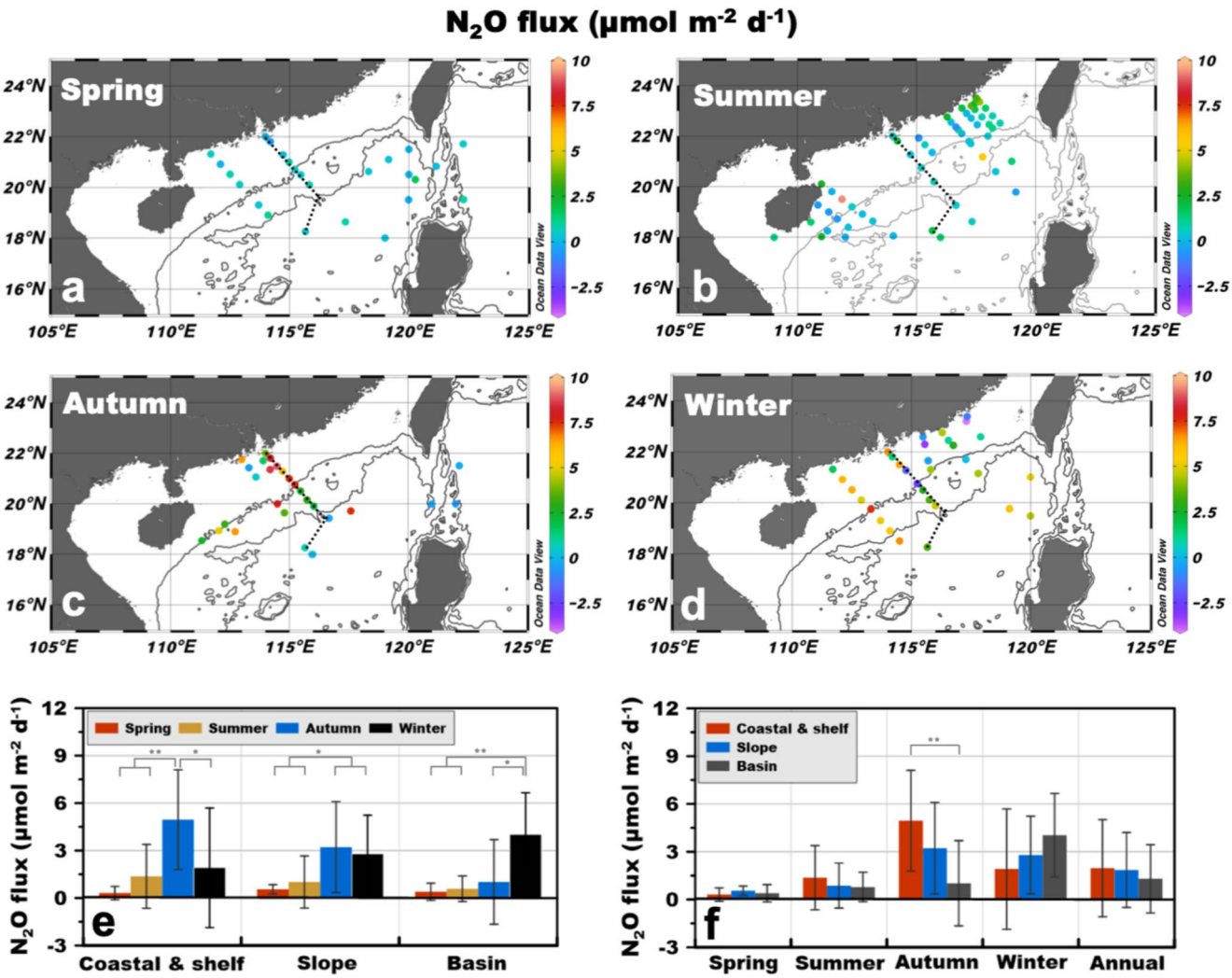

Figure 4. Air-sea fluxes of N_2O in shelf, slope and basin areas at different seasons. (a)–(d) spring, summer, autumn, winter, respectively; (e)–(f) N_2O flux intensity at different seasons and in different regions of the SCS. The black dashed lines in panels (a)–(d) denote transect A. * and ** denote significance at 0.05 and 0.01 levels (*t* test), respectively.

The water column was more stratified in the warm seasons (spring and summer). Accordingly, N_2O, DO, and NO_X^- in the upper mixed layer were lower in spring and summer than in autumn and winter. However, a reversed seasonal correlation was observed in the subsurface water. Below the upper mixed layer, the lowest N_2O and NO_X^- concentrations and the highest DO concentration were measured in winter.

3.4. N_2O Distribution in the Mesopelagic and Bathypelagic Zone

Below the euphotic zone, N_2O concentration increased toward the bottom at the shelf stations, while at the slope and basin stations, a concentration maximum was consistently observed in the mesopelagic layer, coinciding with the DO minimum and NO_X^- maximum layer (Figure 5). Below the N_2O maximum, the N_2O concentration slightly decreased downward and remained near-constant in the deep water. These mirrored vertical distributions between N_2O and DO indicated an intimate relationship between N_2O production and DO consumption.

For the slope and basin stations, the N_2O concentration showed a zonal increasing trend from the Luzon Strait to the SCS in the upper 600 m, accompanied by decreased DO and increased NO_X^- concentrations. The regional differences in N_2O and NO_X^- were less pronounced below the concentration maximum layer. High N_2O concentrations (i.e., ~30 nmol L^{-1}) in the mesopelagic layer (i.e., 600–800 m) were observed in the slope of the NSCS

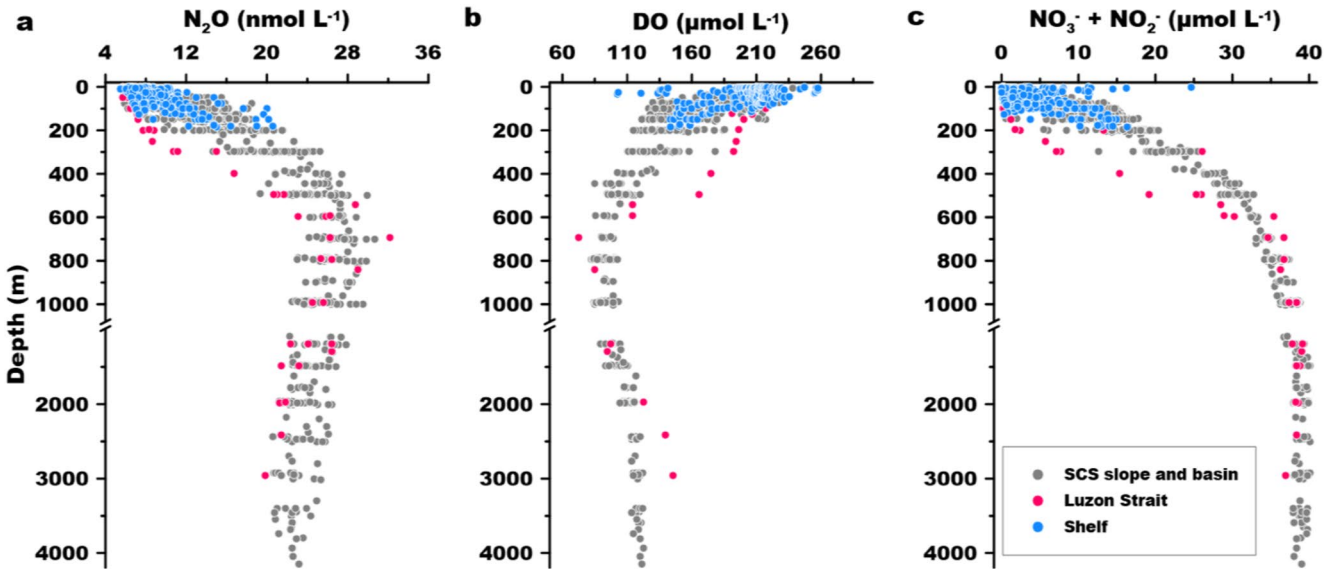

Figure 5. Vertical distributions of N_2O, DO, and NO_X^- concentration. (a) N_2O concentration; (b) DO concentration; (c) NO_X^- concentration.

and at the stations adjacent to the Luzon Strait and were comparable to the peak value (~28–32 nmol L^{-1}) reported in the study area (Tseng et al., 2016; Zhang et al., 2019).

At depths between 100 m and the N_2O concentration maximum, strong positive relationships were observed between ΔN_2O, AOU, and NO_X^- (Figure 7). However, the slopes of the regressions were spatially variable: the slope of ΔN_2O: AOU was lowest (0.05) in the shelf region and highest (0.10) in the Luzon Strait, and intermediate in the SCS basin at 0.08, indicating that the net N_2O yield during DO consumption was highest in the Luzon Strait and lowest in the shelf region (Figure 7a). These values were consistent with previous observations in the NSCS shelf (0.05) (Zhang et al., 2019) and the WPS (0.09) (Tseng et al., 2016). Globally, these ratios fell in the lower range of reported ΔN_2O: AOU values (0.01–0.30) (Capelle et al., 2018; Nevison et al., 2003). Analogously, the slope of ΔN_2O: NO_X^- was lowest in the shelf region (0.35) and highest in the Luzon Strait (0.61) (Figure 7b), close to the reported value in the SCS (0.65) (Han et al., 2013) and the subtropical Atlantic (0.74)

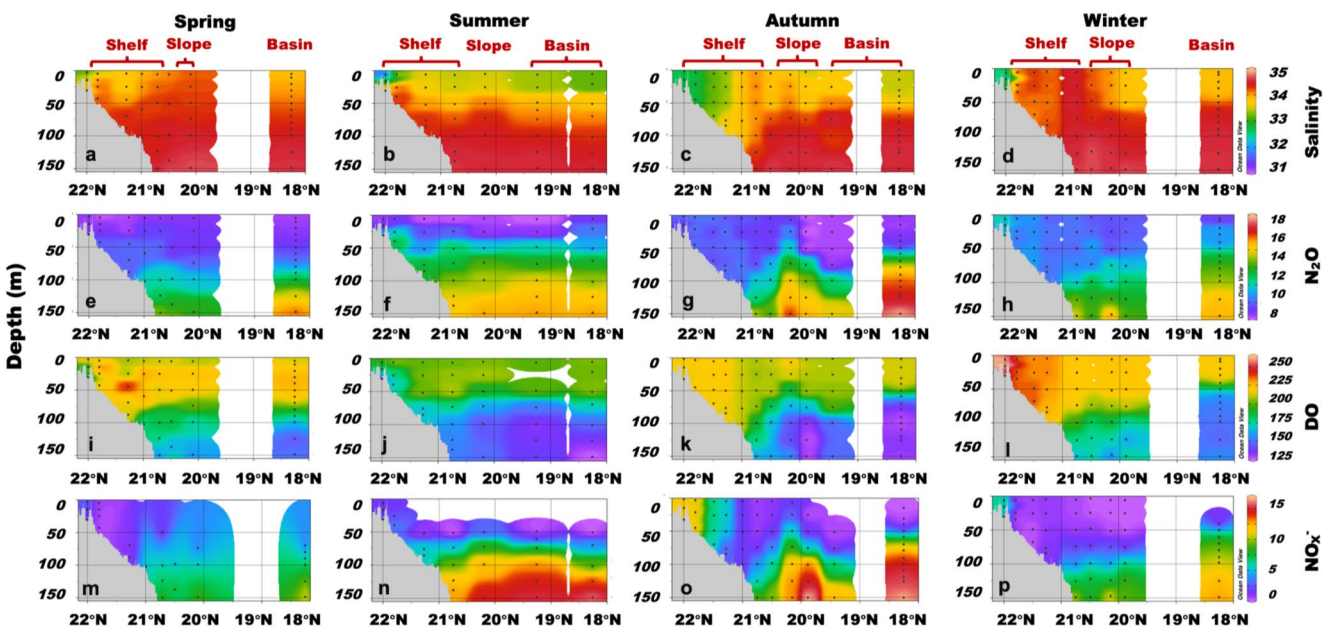

Figure 6. Seasonal distributions of salinity, N_2O, DO and NO_X^- in the upper 150 m along transect A. (a)–(d) salinity; (e)–(h) N_2O; (i)–(l) DO; and (m)–(p) NO_X^-.

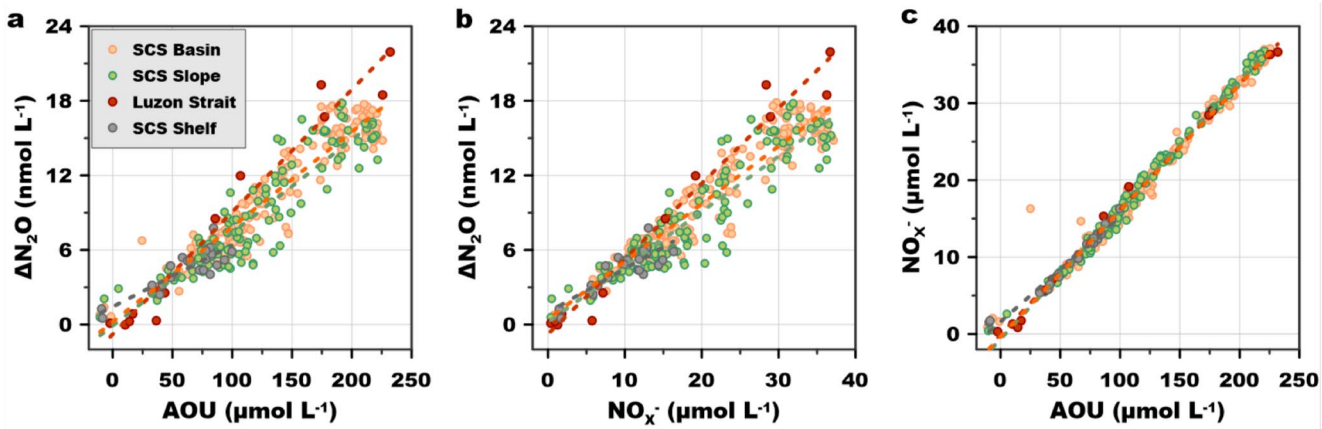

	Slope	Intercept	p
Shelf	0.05±0.01	1.43±0.41	<0.01
Slope	0.08±0.00	-0.08±0.40	<0.01
Basin	0.08±0.00	0.22±0.31	<0.01
Luzon	0.10±0.01	-0.78±0.77	<0.01

	Slope	Intercept	p
Shelf	0.35±0.05	0.98±0.51	<0.01
Slope	0.44±0.02	0.20±0.38	<0.01
Basin	0.46±0.01	0.44±0.29	<0.01
Luzon	0.61±0.03	-0.77±0.68	<0.01

	Slope	Intercept	p
Shelf	0.14±0.01	1.60±0.34	<0.01
Slope	0.17±0.00	-0.65±0.19	<0.01
Basin	0.16±0.00	-0.35±0.28	<0.01
Luzon	0.16±0.00	-0.05±0.43	<0.01

Figure 7. Relationships between excess N_2O, AOU and NO_X^- at the depth range of 100 m to the depth of N_2O maximum in the study area. (a) ΔN_2O: AOU; (b) ΔN_2O: NO_X^-; (c) NO_X^-: AOU. The dashed lines show least square linear regression, the slope, intercept and significance of the correlation are shown in the lower panels.

(Walter et al., 2006). The slope of NO_X^-: AOU ranged from 0.14 to 0.17 (Figure 7c), which was also close to the value reported in the SCS (0.17–0.18) (Tseng et al., 2016; Zhang et al., 2019), the western North Pacific (~0.14) (Yoshida et al., 1989) and the Eastern South Pacific gyre (0.19) (Charpentier et al., 2007).

At depths greater than the N_2O concentration maximum, the positive linear relationship between ΔN_2O and AOU, NO_X^- collapsed; instead a reversed correlation between ΔN_2O and NO_X^- was observed (Figures S5a and S5b in Supporting Information S1); while the positive correlation between NO_X^- and AOU remained (Figure S5c in Supporting Information S1).

4. Discussion

4.1. Spatiotemporal Variability of N_2O Fluxes

Annually, the area weighted average surface N_2O saturation was 107.3 ± 6.0%, suggesting the NSCS was overall a net source of N_2O to the atmosphere. However, both oversaturation and undersaturation were observed in coastal, shelf, and basin regimes. Among the investigated sites, 23% of the stations were undersaturated with respect to atmospheric N_2O whilst 77% of the stations were oversaturated (Figures 3c, 3f, 3i and 3l; Figure S6 in Supporting Information S1). Undersaturated surface N_2O has been observed in the adjacent WPS (Tseng et al., 2016), the shelf and slope of the East China Sea (Chen et al., 2021; Gu et al., 2021), and the Mediterranean Sea (Marty et al., 2001), implying a wide occurrence of N_2O undersaturation in the low latitudinal oceans. The underlying reason for such undersaturation, however, remains unclear. The reduction of nutrient loading (Ma et al., 2019), rapid increase of atmospheric N_2O concentration and climatological variabilities (Gu et al., 2021), and biological N_2O consumption by unidentified diazotrophic cyanobacteria (Cornejo et al., 2015) and N_2O reducing microbes (Sun et al., 2020) could all result in the apparent undersaturation, but the exact mechanism is yet to be elucidated.

The air-sea flux ranged from −2.3 to 9.4 μmol N_2O m^{-2} d^{-1} (area weighted average flux 1.7 ± 1.6 μmol m^{-2} d^{-1}). The areal integrated N_2O fluxes from the shelf, slope and basin were 1.9 ± 1.2 × 10^8, 0.8 ± 0.5 × 10^8, and 1.2 ± 0.7 × 10^8 mol N_2O yr^{-1}, respectively (Table S3 in Supporting Information S1). By comparison, based on the reported annual air-sea CO_2 flux intensity in the NSCS (Dai et al., 2022; Li et al., 2020), estimated CO_2 fluxes in the shelf, slope, and basin areas of the NSCS are −2.1 ± 3.2 × 10^{11} mol yr^{-1}, 0.1 ± 0.7 × 10^9 mol yr^{-1}, and 3.1 ± 0.9 × 10^{11} mol yr^{-1}, respectively. Using a global warming potential at the 100-year time horizon (GWP_{100}, 1 mol N_2O is equivalent to 300 mol CO_2 in retaining radiative energy) (Albritton et al., 1995), the GWP_{100} of N_2O

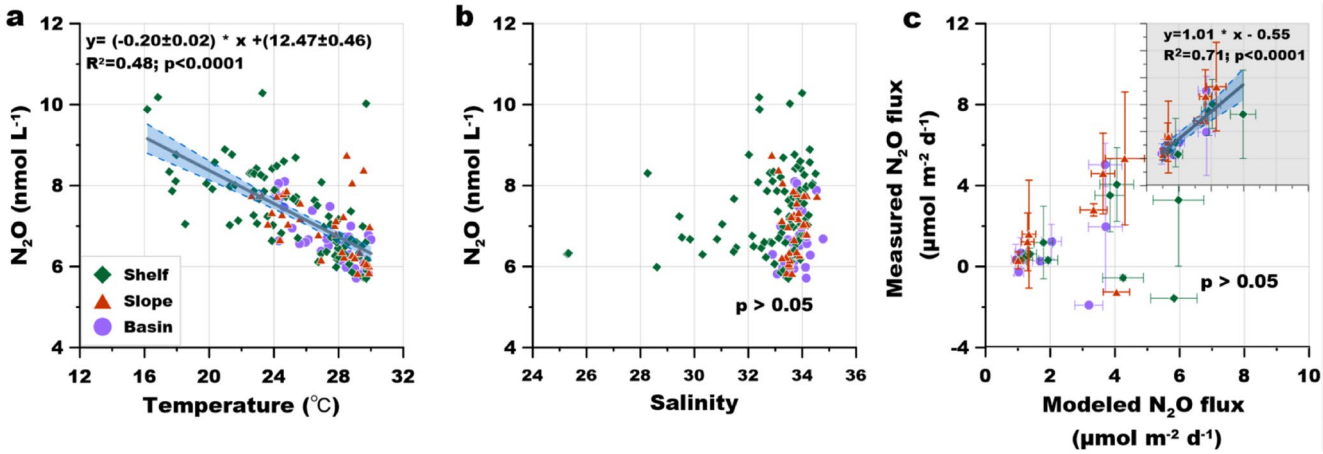

Figure 8. Relationships between surface N_2O and temperature, salinity, and the comparison between N_2O fluxes are derived from the temperature-N_2O concentration relationship-based method and from the measured N_2O-based method. (a) N_2O concentration versus temperature in the surface waters; (b) N_2O concentration versus salinity; (c) comparison of N_2O fluxes using measured and modeled N_2O concentrations, the inset panel shows the relationship after removing the negative flux values. The solid lines show the least square linear regression.

was estimated to be $0.6 \pm 0.4 \times 10^{11}$ mol yr^{-1}, $0.2 \pm 0.1 \times 10^{9}$ mol yr^{-1}, and $0.3 \pm 0.2 \times 10^{11}$ mol yr^{-1}, in the shelf, slope, and basin of the NSCS, respectively. These results showed the N_2O fluxes to the atmosphere would offset 27.8% of the CO_2 sink in the shelf region and are equivalent to 248.9% and 23.1% of the CO_2 emission in the slope and basin of the NSCS, respectively. Taking the NSCS as a whole, the GWP_{100} of N_2O emission is estimated to be 73.8% of that of the CO_2 flux (Table S4 in Supporting Information S1). This comparison not only reveals the significance of N_2O in offsetting the benefit of marine carbon sequestration but also shows that N_2O is a key component for future study to complete the knowledge gaps associated with the marginal seas in the global climatic system.

Prominent seasonal variability (Figures S4a–S4c in Supporting Information S1) of air-sea N_2O fluxes was observed in our study, and the spatial variation was less pronounced (Figures S4d–S4f in Supporting Information S1). The highest area weighted average flux occurred in autumn (3.2 ± 1.8 μmol m^{-2} d^{-1}), followed by winter (2.9 ± 1.9 μmol m^{-2} d^{-1}) and summer (0.9 ± 1.0 μmol m^{-2} d^{-1}), while the lowest flux was observed in spring (0.4 ± 0.3 μmol m^{-2} d^{-1}). These air-sea fluxes were at the lower end of the reported N_2O flux in the NSCS (1.1 ± 1.0 to 11.3 ± 6.8 μmol m^{-2} d^{-1}) (Han et al., 2013; Tseng et al., 2016; Zhang et al., 2019), but were slightly higher than the values reported in the subtropical gyre of the Western North Pacific (0.7–0.9 μmol m^{-2} d^{-1}) (Breider et al., 2015); station ALOHA (0.5 ± 0.9 μmol m^{-2} d^{-1}) (Wilson et al., 2017), the subtropical North Atlantic ocean (0.4–1.1 μmol m^{-2} d^{-1}) (Forster et al., 2009), or the global average of subtropical gyres (0.24 ± 0.05 μmol m^{-2} d^{-1}) (Yang et al., 2020). These comparisons suggest that the NSCS acts as a weak source of N_2O to the atmosphere in the spring and summer, similar to the subtropical gyre regions and is a moderate source with the flux level similar to tropical and high latitude oceans in the autumn and winter. Regionally, the shelf was the largest contributor in summer and autumn, and the basin represented the main source in winter and spring (Table S3 in Supporting Information S1). This first report revealing the significant seasonality of N_2O fluxes in the SCS echoes recent initiatives of increasing time-series N_2O observation to better constrain the marine N_2O budget (Bange et al., 2019; Yang et al., 2020).

In our study, the surface N_2O concentration was highly correlated with temperature ($p < 0.01$) (Figure 8a); such a tight relationship between temperature and N_2O concentration is consistent with the finding at station ALOHA where the seasonality of the surface N_2O distribution was largely influenced by seasonal temperature oscillations (Wilson et al., 2017). Temperature is a fundamental control on N_2O distribution by exerting direct influence on biological N_2O cycling (e.g., nitrification and denitrification) and by regulating the solubility and equilibrium of N_2O in seawater. In our study, temperature explained ~48% of the variance in N_2O concentrations (Figure 8a). Note that such correlations do not apply to salinity, implying that the variation of N_2O concentrations was not directly related to the changes in water masses (Figure 8b).

The strong correlation between N_2O concentrations and temperature suggest a potential to use temperature to predict N_2O concentrations and/or ΔN_2O, which could allow extrapolations of the measurements. We therefore investigated such potentials by using our observed temperature-N_2O concentration relationship (Figure 8a), and the satellite-derived sea surface temperature, salinity, and wind speed in our study area following Li et al. (2020). Upon the predicted surface N_2O concentrations, we computed the fluxes based on the ΔN_2O and wind speed at a given region (shelf, slope and basin) and in the sampling month. Our results showed that the computed N_2O fluxes were not consistently correlated with the observed fluxes, primarily because the model failed to reproduce the negative fluxes, leading to large errors for the samples with undersaturated N_2O concentration (Figure 8c). However, the predicted results and observed fluxes were highly correlated when the negative fluxes were removed (i.e., the undersaturated samples) (Figure 8c, inset panel), indicating that the empirical relationship between the temperature and N_2O concentration is in order for predicting surface fluxes when N_2O is oversaturated. However, cares must be taken in deriving the regional temperature–N_2O relationship and computing the fluxes in waters with undersaturated N_2O.

To assess whether any interannual variability of surface N_2O distribution and flux can be detected during our study period, we grouped our data set into warm (spring and summer, six cruises) and cold (autumn and winter, four cruises) seasons. For the warm seasons, the distribution of N_2O concentrations, saturation and fluxes were relatively stable except for September 2008 in the Luzon Strait area, featuring higher surface temperature and salinity, and lower NO_X^- and N_2O concentrations than the NSCS in the surface layer (Figure 5; Figures S7a–S7e in Supporting Information S1). The low N_2O concentration and flux observed in September 2008 were thus more likely attributed to the spatial difference between Luzon Strait and the NSCS rather than inter-seasonal variations. For the cold seasons, a clear increase in temperature accompanied by a slight decrease in salinity was observed. However, it should be noted that the cruise in 2012 was carried out between late September and October representing a transitional period between warm and cold seasons. The N_2O concentration was highest during the cruise of January 2010, and the concentrations were comparable between the remaining three cruises. By contrast, an increasing trend of N_2O saturation can be found from 2009 to 2012 that covaried with the temperature. The N_2O fluxes, on the other hand, were significantly higher in the 2010 cruises than in the 2009 winter cruise, but slightly decreased from 2010 to 2012 (Figures S7f–S7j in Supporting Information S1). We thus contend that a clear interannual trend in the warm seasons cannot be discerned in our data, but an increasing trend of N_2O saturation can be found in the cold seasons despite the fact that the N_2O concentration remains unchanged. Time-series observations with a higher temporal resolution are warranted to confirm the seasonal trend and to address the key question of interannual N_2O flux variability.

4.2. Temporal Variability of N_2O Distribution in the Euphotic Zone

Repeated surveys at transect A at all four seasons allowed examination of the seasonality of N_2O distribution in the euphotic zone of the NSCS. Due to the higher freshwater discharge rate in the warm and wet season (summer and autumn), higher amounts of nutrients are delivered from the terrestrial source into the coastal zone (Chen et al., 2001; Wong et al., 2007). Consequently, the depth-integrated NO_X^- (surface to bottom depth) in the coastal and shelf region was higher in autumn (0.4 ± 0.1 mol m^{-2}) than in spring (0.2 ± 0.3 mol m^{-2}), while other seasonal differences were not significant (Figure S8a in Supporting Information S1). At the slope and basin stations, the integrated NO_X^- in the upper 150 m water column was significantly higher in autumn (1.1 ± 0.3 mol m^{-2}) than in winter (0.6 ± 0.3 mol m^{-2}) (Figure S8b in Supporting Information S1). However, different from the shelf stations, the lower nutrient inventory in the upper layer of the NSCS basin in the winter was caused by the stronger intrusion of the KC, which is characterized by ultra-oligotrophic waters, resulting in dilution of nutrient inventories (Du et al., 2013).

In contrast to the seasonal differences in depth-integrated NO_X^-, no significant seasonal difference in the N_2O inventory was found in either shelf or basin waters (Figures S8c and S8d in Supporting Information S1). Decreasing seawater temperature in the cold seasons increases the solubility of N_2O, leading to a higher surface N_2O concentration due to equilibration across the air-sea interface. In contrast to the seasonality of surface N_2O distribution, the concentration in the lower euphotic zone was higher in the warm seasons than the cold seasons, probably because the stronger stratification in the warm seasons impeded the upward diffusion of N_2O from the lower euphotic zone into the surface mixed layer, leading to accumulation of N_2O in the euphotic zone during the warm seasons. As a result, the depth-integrated N_2O inventory in the water column was comparable among the four

seasons. These results suggest a crucial role of temperature and stratification in regulating the distribution and inventory of N_2O in the NSCS.

Trophic status is generally considered as a primary control on N_2O production and distribution in the aquatic system (Naqvi et al., 2010; Yang et al., 2020). The spatial-seasonal variation of NO_X^- and N_2O, however, did not follow the same pattern in our study, implying different and complex controls on nutrient and N_2O distributions in the NSCS. For the shelf region, freshwater discharge plays a key role in controlling seasonal nutrient distribution, while temperature likely dominates the N_2O distribution in shallow water. In the open water of the NSCS, the strength of KC intrusion largely controls the seasonal evolution of nutrient distribution (Du et al., 2013); however, different from NO_X^- distribution, the dilution effect of the KC on N_2O was not found in the winter and spring seasons. Several recent studies point out the stimulation of organic carbon and nitrogen remineralization in the mixing zone of KC and NSCS (Huang et al., 2019; Li et al., 2021), which increases the ammonia supply (Zhu et al., 2021) and facilitates ammonia oxidation (Xu et al., 2018). Moreover, the reduced stratification in the winter might favor supplies of subsurface nutrients into the surface ocean, resulting in higher primary productivity in winter than summer (Chen et al., 2006; Tseng et al., 2005). The enhanced biological productivity and nitrogen regeneration during winter thus might compensate the N_2O inventory via biological N_2O production, revealing a complex physical-biological interactive control on the N_2O distribution in the NSCS.

4.3. Sources and Distribution of N_2O in the Water Column

4.3.1. N_2O Source in the Euphotic Layer (0–100 m)

To avoid potential biases caused by the in-situ O_2 production and air-sea mixing processes, the AOU above 100 m of the water column was excluded from our analysis. Biological N_2O production in the euphotic zone has historically been less studied due to the long-held recognition that denitrification is blocked by high ambient DO concentration and nitrification is inhibited by light (Horrigan et al., 1981; Olson, 1981). However, active nitrification and N_2O production have recently been reported in the global sunlit ocean (Ji and Ward, 2017; Shiozaki et al., 2016; Wan et al., 2018), raising the necessity of revisiting the source of N_2O in the euphotic zone.

Using a one-dimensional advection-diffusion model (Du et al., 2017), we computed the upward flux of N_2O across 100 m at the SEATs station. The estimated vertical N_2O flux at 100 m was 0.26 ± 0.11 μmol N_2O m^{-2} d^{-1} (range 0.20–0.41 μmol N_2O m^{-2} d^{-1}). By comparison, the estimated air-sea N_2O flux at the same station was 1.65 ± 1.13 μmol N_2O m^{-2} d^{-1} (range 0.48–3.35 μmol N_2O m^{-2} d^{-1}). The difference between the upward flux and air-sea flux indicates that as much as 84.3% of N_2O in the upper 100 m was produced locally, that is, within the top 100 m, assuming a steady state, which was consistent with the estimate of 70% at station ALOHA (Wilson et al., 2017) and 70%–75% for the tropical Atlantic Ocean (Kock et al., 2012). Although the one-dimensional model was not applicable in the shelf and Luzon Strait areas due to active lateral transport (Zhu et al., 2019), a recent investigation of N_2O isotopes in the shelf and slope of the NSCS shows that a large N_2O source could be revealed in the lower euphotic zone in the study area (Zhang et al., 2019). We thus suggest a large fraction of the N_2O that sustains the air-sea flux results from in-situ production within the euphotic zone in the NSCS.

4.3.2. N_2O Distribution in the Subsurface and Intermediate Water (100 m to Depth of N_2O Maximum)

Linear regression analysis between ΔN_2O, AOU, and NO_3^- is widely used to probe the source of N_2O in the ocean. A strong positive linear relationship between ΔN_2O and AOU has been extensively observed in nearly all ocean provinces outside the oxygen minimum zones (Cohen and Gordon, 1979; de la Paz et al., 2017; De Wilde and Helder, 1997; Freing et al., 2009; Nevison et al., 1995, 2003; Tseng et al., 2016; Walter et al., 2006; Yoshinari, 1976). This relationship is usually taken as an evidence of N_2O production through nitrification, an obligately aerobic process that converts NH_4^+ to NO_3^-. Consistent with those results, significant correlations were observed between ΔN_2O, AOU, and NO_x^- in our study in the depth range between 100 m and the depth of the N_2O concentration maximum, although with significantly different slopes in different regions (Figure S5 in Supporting Information S1). Likewise, the ratio ΔN_2O: NO_X^- also varied significantly among regions (Figure S5 in Supporting Information S1). The identical spatial patterns between ΔN_2O: NO_X^- and ΔN_2O: AOU suggests that the spatial variation of these ratios was controlled by similar processes.

Several hypotheses have been proposed to explain the regional and vertical differences of ΔN_2O: AOU, including differences in N_2O production processes (De Wilde and Helder, 1997; Law and Owens, 1990), the impact of

mixing and advection (de la Paz et al., 2017; Nevison et al., 2003), variable N_2O yield during nitrification under different ambient DO concentrations (Capelle et al., 2018; Nevison et al., 2003) and the potential effect of temperature and pressure on N_2O yield (Freing et al., 2009; Walter et al., 2006). The rate of most microbial metabolisms increases with temperature, thus both N_2O production and O_2 consumption rates are temperature dependent, but the net effect on ΔN_2O: AOU remains unclear (Nevison et al., 2003). It is suspected that the general decline in temperature with depth leads to the decrease of N_2O production and O_2 consumption rate but not for the ΔN_2O: AOU ratio because both these rates are controlled by the aerobic organic remineralization process when the ambient DO is sufficient (Freing et al., 2009; Walter et al., 2006). To our knowledge, there is no direct experimental evidence quantifying the impact of pressure on the relationship between N_2O production and O_2 consumption to date, although the pressure effect has been hypothesized in explaining the reduced ΔN_2O: AOU in the deep ocean (Butler et al., 1989). Moreover, temperature and pressure effects are hard to separate because these two factors covary with depth in the ocean. In our study, the slopes of both ΔN_2O: AOU and ΔN_2O: NO_X^- varied among sampling areas (i.e., shelf vs. SCS slope and basin vs. Luzon Strait), while the slopes did not change over depth and temperature within area (Figure 7; Figure S9 in Supporting Information S1), suggesting the effect of temperature and pressure was not the primary determinant on the observed ΔN_2O: AOU relationships in our study.

DO concentration is a fundamental control on N_2O production through either nitrification or denitrification. During nitrification, the N_2O yield increases rapidly as DO decreases at low DO concentrations, that is, from 0.5 to 10 μmol L^{-1} (Frame and Casciotti, 2010; Goreau et al., 1980; Ji et al., 2018; Qin et al., 2017). Denitrification is enhanced at low DO concentrations but the net effect of DO on N_2O accumulation is complex. The DO threshold for net N_2O production is estimated to range from 2 to 20 μmol L^{-1}, but net consumption of N_2O by denitrification occurs when DO drops to <2 μmol L^{-1} (Babbin et al., 2015; Brandes et al., 2007; Ji et al., 2018). Although the specific threshold appears to be site and microbial species dependent and remains uncertain, regulation by DO of N_2O production is most important at low DO concentration (i.e., <20 μmol L^{-1}). Above this threshold, the denitrification process is inhibited, and N_2O yield during nitrification is no longer sensitive to the change in DO. On the other hand, several lines of evidence indicate that N_2O in oxygenated water could be produced via multiple pathways, such as nitrifier denitrification and denitrification in the particle associated micro-environment, expanding the niche of anaerobic N_2O production to the oxygenated ocean (Breider et al., 2015; Frame et al., 2014; Ostrom et al., 2000; Popp et al., 2002; Zhang et al., 2019). In principle, the involvement of nitrifier denitrification and denitrification pathways would (a) elevate the apparent ΔN_2O: AOU as these N_2O production processes do not consume DO, (b) increase ΔN_2O: NO_X^- by increasing both N_2O production and NO_X^- consumption, and (c) reduce ΔN_2O: NO_X^- if net N_2O consumption occurred in the anoxic core of the large particles. Substantial contribution by nitrifier-denitrification to N_2O production has been suggested in the intermediate water of station ALOHA (i.e., >40%–75% of N_2O at ~300 m) (Popp et al., 2002) and the Northwest Pacific (i.e., >30%–55% of N_2O at ~140 m) (Breider et al., 2015) based on the finding of decreased isotope values (isotope minima) of N_2O at these depths. By contrast, the contribution of nitrifier-denitrification to N_2O in the intermediate water of SCS is significantly lower than those observations (i.e., >70% of N_2O is produced through hydroxylamine oxidation in the intermediate water of SCS) (Zhang et al., 2019). Variable N_2O production by nitrifier-denitrification might partially explain the higher ΔN_2O: AOU in the intermediate water of the Western Pacific stations than the SCS stations. Nitrifier-denitrification is typically associated with ammonia oxidizing bacteria (AOB), but AOB have rarely been detected in the water column of open ocean systems, raising the question of which microbes are responsible for the observed "nitrifier-denitrification" like pathway. On the other hand, accumulating evidence shows the marine ammonia oxidizing archaea (AOA), which produce N_2O by a pathway that is distinct from their bacterial counterparts by incorporating NO_2^- (and/or intermediates from NO_2^-) into N_2O (Kozlowski et al., 2016; Stieglmeier et al., 2014), likely dominate NH_4^+ oxidation and N_2O production in the ocean (Buitenhuis et al., 2018; Freing et al., 2012; Ji et al., 2018). Moreover, a recent study reveals the capability of marine AOA to produce N_2O under anoxic conditions (Kraft et al., 2022). However, it remains to be elucidated whether AOA are capable of producing N_2O in the absence of DO consumption in oxic water (i.e., can they facilitate certain abiotic N_2O formation reactions by releasing intermediates such as NO into the environment), and to what extent AOA could contribute to the N_2O isotope minima in the water column. Moreover, due to the stronger vertical mixing and upwelling in the SCS (Wong et al., 2007; Zhu et al., 2019), a higher fraction of SCS deep-water (characterized by lower ΔN_2O and higher AOU, Figure S5 in Supporting Information S1) would mix into the intermediate layer, which might reduce its ΔN_2O: AOU.

Counterintuitively, the ΔN_2O: AOU on the shelf was significantly lower than in the basin stations in our study. Because the primary productivity and particle content are higher in the shelf region than in the slope and basin (Cai et al., 2015; Wong et al., 2007), a higher ΔN_2O: AOU would be expected due to the more favorable environment for nitrifier-denitrification in the shelf region. Potential causes of the apparent low ΔN_2O: AOU in the shelf regions include low N_2O production efficiency, high DO consumption, and N_2O consumption. Compared to the open water stations, the shelf stations receive more terrestrial organic matter, which is characterized by higher carbon: nitrogen ratio than the autochthonous organics (Huang et al., 2017; Li et al., 2017). Consequently, lower ΔN_2O: AOU might be expected due to the higher O_2 requirement to provide the same amount of NH_4^+. Likewise, the remineralization of organic matter in surface sediment might also lead to higher O_2 consumption: NH_4^+ production ratio. Moreover, complete denitrification or N_2O consumption in the anoxic core of marine aggregates, and the sediment (Klawonn et al., 2015; Stief et al., 2016; Wyman et al., 2013) could also lead to low ΔN_2O: AOU. The potential consumption of N_2O in bottom water of the shelf region is also evidenced by the elevated N_2O isotopic signal in the NSCS (Zhang et al., 2019). Meanwhile, intensive DO uptake by the sediment has been reported in the coast and shelf region of the NSCS and the East China Sea (Cai et al., 2014; Zhang and Li, 2000), which might contribute to the low ΔN_2O: AOU. Therefore, we attribute the observed low ΔN_2O: AOU in the shelf regions to the combined effects of the higher O_2 consumption: NH_4^+ production ratio of the terrestrial and sedimentary sourced organic matter than the marine autochthonous organics and N_2O consumption in anoxic microenvironments and sediment.

Although the NSCS receives a substantial amount of NO_X^- from runoff (Chen et al., 2001) and atmospheric deposition (Kim et al., 2014), the ratio of NO_x^-: AOU in the shelf was comparable with the ratio in the slope and open waters, and was less variable than the ratio ΔN_2O: AOU (Figure 7). The absence of significant regional difference of NO_x^-: AOU was likely due to the fact that these allochthonous NO_X^- sources were supplied directly to the surface ocean and were efficiently scavenged by the phytoplankton, which is consistent with the high NO_3^- assimilation rate on the shelf of NSCS (Lee Chen, 2005; Ning et al., 2004). Consequently, the NO_X^- below the euphotic zone would be mainly produced by nitrification through the particulate organic matter (POM) remineralization. This tight link to nitrification establishes a more direct connection between NO_X^- production and DO consumption than that between ΔN_2O and AOU. Assuming the NH_4^+ accessed by nitrifiers was solely sourced from the POM with composition in the redfield ratio, the NO_3^- production process in principle accounts for 23% of total DO consumption during the complete remineralization process. However, the observed NO_X^-: AOU value in our study, as well as other ocean provinces, was consistently lower than the predicted value (0.23) following the redfield ratio. NO_X^-: AOU ratio systematically lower than the theoretical value observed in the global ocean implies that a considerable fraction of NO_3^- was removed or the NH_4^+ sourced from organic decomposition was consumed by other microorganisms rather than being oxidized by nitrifiers. In our study, the minimum DO concentration in the water column was higher than 60 μmol L^{-1}, suggesting that NO_x^- removal through denitrification was not likely a main cause for the low ratio of NO_X^-: AOU, although NO_X^- removal in the oxic water could not be fully excluded. On the other hand, several recent studies report high NH_4^+ utilization rates by heterotrophic prokaryotes (Deng et al., 2021; Trottet et al., 2016) and chemolithotrophs (Guerrero-Feijóo et al., 2018; Pachiadaki et al., 2017; Zhang et al., 2020) in the global dark ocean, suggesting at least part of the NH_4^+ was consumed to produce microbial biomass rather being oxidized by nitrifiers. The average NO_X^-: AOU ratio of 0.16 in our study suggests that 70% (0.16/0.23) of NH_4^+ was oxidized and 30% was used for assimilation in the dark ocean.

4.3.3. N_2O Distribution in the Deep Water (>the Depth of N_2O Maximums)

Below the N_2O maximum in the slope and basin, the positive relationship between ΔN_2O, AOU and NO_X^- collapsed, likely due to the lack of variation and small range in all three parameters. The lack of positive relationships observed in the mesopelagic layer was previously attributed to the pressure effect at the greater depth, that is, the production of N_2O was inhibited by high pressure in the deep water during DO consumption processes, leading to the deviation of the linear relationship between ΔN_2O and AOU, but direct experimental evidence remains lacking (Butler et al., 1989; Nevison et al., 2003). The mixing of water masses (i.e., the deep water in western Subtropical North Pacific and the intermediate water of SCS), which carry distinct ΔN_2O, AOU and NO_X^- signals, might also result in the observed nonlinear relationship. The negative relationship between ΔN_2O and NO_X^- in the deep layer might also reflect a net consumption of N_2O during the NO_X^- accumulation process over the aging of the water mass. Recently, N_2O reductase functional genes (*nosZ* clade II) belonging to non-canonical denitrifiers were identified in oxygenated waters (Bertagnolli et al., 2020; Sun et al., 2017). Clade

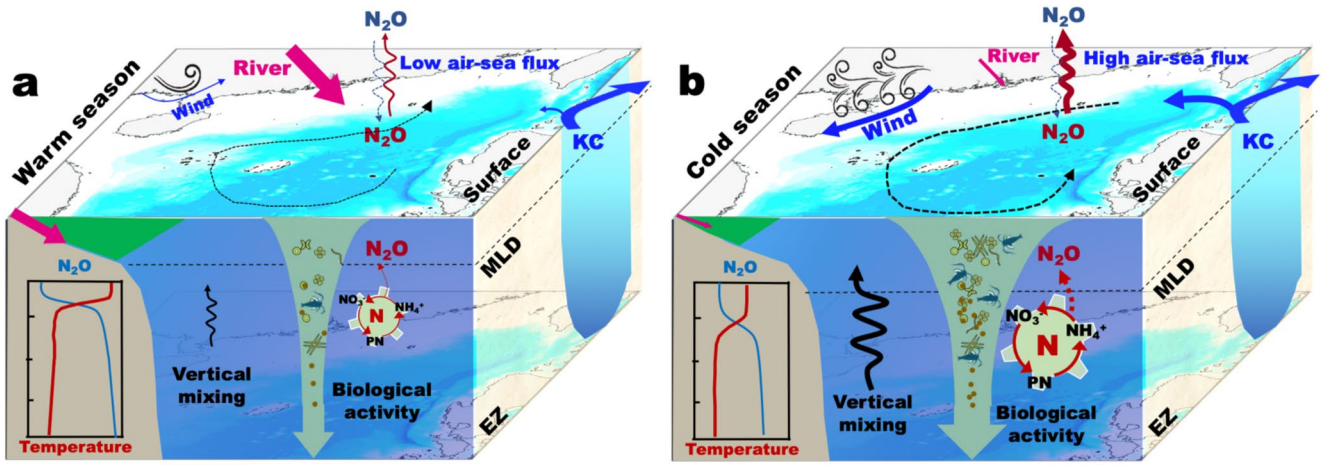

Figure 9. Summary of the key processes and controls on the seasonality of air-sea N_2O flux and N_2O distribution in the euphotic zone of the NSCS. (a) Warm season and (b) cold season. Seasonality of surface N_2O concentration is regulated mainly by temperature, and the air-sea N_2O flux is determined by both temperature and wind. In the water column, riverine discharge induces higher nutrient and N_2O levels on the shelf in the summer; while the extent of stratification and KC intrusion regulate the vertical distribution of nutrient and N_2O inventory in the basin of the NSCS.

II *nosZ* genes are often found in microbes that do not perform the complete denitrification pathway, indicating a potential N_2O consumption pathway in the oxic water i.e., not coupled to NO_3^- reduction. If N_2O consumption occurred, it could lead to the negative ΔN_2O: NO_X^- in the deep water. However, the activity of *nosZ* clade II in the oxic deep water has rarely been investigated and warrants further exploration.

Together, our findings demonstrate both the utility and the complexity of interpreting ΔN_2O, AOU, NO_X^- relationships to understand the source and production of N_2O in the ocean. A three-layer structure was proposed here: (a) in the euphotic zone, the ΔN_2O: AOU and ΔN_2O: NO_X^- relationships were masked by vigorous air-sea flux and biological O_2 production and NO_X^- consumption; (b) in the mesopelagic ocean, the spatially variable ΔN_2O: AOU and ΔN_2O: NO_X^- could be attributed to additional N_2O production processes such as nitrifier-denitrification and the impact of water mixing in the oxygenated open ocean. In the coastal and shelf region, the role of sediment and the heavy particle loading should be accounted for to better understand the observed ΔN_2O: AOU; (c) the absence of strong positive relationships between ΔN_2O, AOU and NO_X^- in the deep ocean reflects lower biological activity and indicates a potential role of physical mixing in masking the biological signal. However, the extent to which the relationship was regulated by biological N_2O cycling processes remains to be addressed. Given that ΔN_2O: AOU and ΔN_2O: NO_X^- ratios are widely used in the parameterization of biogeochemical models related to N_2O production and flux (Buitenhuis et al., 2018; de la Paz et al., 2017; Freing et al., 2009; Nevison et al., 2003), our study suggests caution in extrapolating N_2O production by simply using a fixed ΔN_2O: AOU ratio.

5. Conclusions

Based on the data collected from 10 cruises covering four seasons in seven consecutive years, we provide robust evidence showing the significant seasonality of surface N_2O distribution and flux in the NSCS. The NSCS overall is a net source of N_2O despite the fact that surface water at >20% of stations was consistently undersaturated. Temperature and wind were the key controls of surface N_2O distribution and air-sea flux in the NSCS. N_2O distribution in the water column also demonstrates significant seasonal variability. Riverine discharge largely regulates N_2O distribution in the coastal and shelf region, while the extent of stratification and KC intrusion into the NSCS and the subsequent biological responses determine the seasonality of N_2O distribution in the open water stations (Figure 9).

Although vigorous mixing and biological O_2 production preclude the application of ΔN_2O: AOU analysis in surface waters, our 1-D mixing model suggests a large fraction of air-sea N_2O might be sustained by local sources in the surface ocean. Below the euphotic zone, the significantly different ΔN_2O, AOU, NO_X^- relationships between regions and depths suggest the complexity of N_2O cycling and its distribution in the ocean. These

differences imply caution when using ΔN_2O, AOU, NO_X^- relationships to evaluate biogeochemical processes. Sources of N_2O in addition to nitrification, along with the impact of physical mixing, should be considered in interpreting the observed ΔN_2O, AOU, NO_X^- relationships.

The importance and benefits of time-series observation have been demonstrated for CO_2 measurements in the global ocean (Bakker et al., 2016; Dai et al., 2022). Similar efforts should be taken to better understand the natural variability of N_2O in the ocean, such as resolving the interannual and intra-seasonal variability and impact of events (upwellings, tropical cyclones) on air-sea exchange (Li et al., 2020), and in turn, to improve our ability to predict the air-sea flux of N_2O in a changing ocean. The present study reveals the significant seasonality of N_2O distribution and flux in the NSCS, establishing a baseline to understand the spatial-seasonal variability of N_2O in the NSCS and to compare with other ocean margins. Even this relatively high-resolution data set, however, was not sufficient to detect interannual differences in fluxes, indicating that longer and more detailed time series observations will be necessary to evaluate interannual trends in the coastal ocean.

Conflict of Interest

The authors declare no conflicts of interest relevant to this study.

Data Availability Statement

All data needed to evaluate the conclusions in the paper are deposited in Zenodo database that can be accessed through https://doi.org/10.5281/zenodo.6672505.

Acknowledgments
This work was supported by the National Natural Science Foundation of China through grants 41890802, 42188102, 92058204, 41721005, and 41706086. We are grateful to the help of Lifang Wang, Tao Huang, Yanping Xu, Chuanjun Du, Xiao Huang, Aiqin Han, Xianghui Guo, and Liguo Guo for the sampling during the research cruises and for nutrient, DO measurements. We also thank Hua-Xia Sheng for creating part of the figures. The crew of R/V Dongfanghong II and Shiyan III are acknowledged for their assistance in sample collection.

References

Albritton, D., Derwent, R., Isaksen, I., & Wuebbles, L. M. (1995). Radiative forcing of climate change. In J. T. Houghton, L. G. Meira Filho, B. A. Callander, N. Harris, A. Kattenberg, & K. Maskell (Eds.), *Climate change: The science of climate change*, (pp. 118–131). Cambridge University Press.

Arévalo-Martínez, D. L., Kock, A., Loscher, C. R., Schmitz, R. A., & Bange, H. W. (2015). Massive nitrous oxide emissions from the tropical South Pacific Ocean. *Nature Geoscience*, *8*, 530–533. https://doi.org/10.1038/Ngeo2469

Babbin, A. R., Bianchi, D., Jayakumar, A., & Ward, B. B. (2015). Rapid nitrous oxide cycling in the suboxic ocean. *Science*, *348*, 1127–1129. https://doi.org/10.1126/science.aaa8380

Bakker, D. C. E., Pfeil, B., Landa, C. S., Metzl, N., O'Brien, K. M., Olsen, A., et al. (2016). A multi-decade record of high-quality fCO_2 data in Version 3 of the Surface Ocean CO_2 Atlas (SOCAT). *Earth System Science Data*, *8*, 383–413. https://doi.org/10.5194/essd-8-383-2016

Bange, H. W. (2006). Nitrous oxide and methane in European coastal waters. *Estuarine, Coastal and Shelf Science*, *70*, 361–374. https://doi.org/10.1016/j.ecss.2006.05.042

Bange, H. W., Arévalo-Martínez, D. L., delaPaz, M., Farías, L., Kaiser, J., Kock, A., et al. (2019). A harmonized nitrous oxide (N_2O) ocean observation network for the 21st Century. *Frontiers in Marine Science*, *6*, 157. https://doi.org/10.3389/fmars.2019.00157

Barnes, J., & Upstill-Goddard, R. C. (2011). N_2O seasonal distributions and air-sea exchange in UK estuaries: Implications for the tropospheric N_2O source from European coastal waters. *Journal of Geophysical Research: Biogeosciences*, *116*, G01006. https://doi.org/10.1029/2009jg001156

Battaglia, G., & Joos, F. (2018). Marine N_2O emissions from nitrification and denitrification constrained by modern observations and projected in multimillennial global warming simulations. *Global Biogeochemical Cycles*, *32*, 92–121. https://doi.org/10.1002/2017gb005671

Bertagnolli, A. D., Konstantinidis, K. T., & Stewart, F. J. (2020). Non-denitrifier nitrous oxide reductases dominate marine biomes. *Environmental Microbiology Reports*, *12*, 681–692. https://doi.org/10.1111/1758-2229.12879

Brandes, J. A., Devol, A. H., & Deutsch, C. (2007). New developments in the marine nitrogen cycle. *Chemical Reviews*, *107*, 577–589. https://doi.org/10.1021/cr050377t

Breider, F., Yoshikawa, C., Abe, H., Toyoda, S., & Yoshida, N. (2015). Origin and fluxes of nitrous oxide along a latitudinal transect in Western North Pacific: Controls and regional significance. *Global Biogeochemical Cycles*, *29*, 1014–1027. https://doi.org/10.1002/2014gb004977

Breider, F., Yoshikawa, C., Makabe, A., Toyoda, S., Wakita, M., Matsui, Y., et al. (2019). Response of N_2O production rate to ocean acidification in the Western North Pacific. *Nature Climate Change*, *9*, 954–958. https://doi.org/10.1038/s41558-019-0605-7

Buitenhuis, E. T., Suntharalingam, P., & Le Quéré, C. (2018). Constraints on global oceanic emissions of N_2O from observations and models. *Biogeosciences*, *15*, 2161–2175. https://doi.org/10.5194/bg-15-2161-2018

Butler, J. H., Elkins, J. W., Thompson, T. M., & Egan, K. B. (1989). Tropospheric and dissolved N_2O of the West Pacific and East Indian Oceans during the El Niño southern oscillation event of 1987. *Journal of Geophysical Research: Atmospheres*, *94*, 14865–14877. https://doi.org/10.1029/JD094iD12p14865

Cai, P., Shi, X., Moore, W. S., Peng, S., Wang, G., & Dai, M. (2014). ^{224}Ra:^{228}Th disequilibrium in coastal sediments: Implications for solute transfer across the sediment-water interface. *Geochimica et Cosmochimica Acta*, *125*, 68–84. https://doi.org/10.1016/j.gca.2013.09.029

Cai, P., Zhao, D., Wang, L., Huang, B., & Dai, M. (2015). Role of particle stock and phytoplankton community structure in regulating particulate organic carbon export in a large marginal sea. *Journal of Geophysical Research: Oceans*, *120*, 2063–2095. https://doi.org/10.1002/2014JC010432

Canadell, J. G., Monteiro, P. M. S., Costa, M. H., Cotrim da Cunha, L., Cox, P. M., Henson, A. V. S., et al. (2021). Global carbon and other biogeochemical cycles and feedbacks. In V.Masson-Delmotte, P. Zhai, A. Pirani, S. L. Connors, C. Péan, S. Berger, et al. (Eds.), *Climate Change 2021: The Physical Science Basis. Contribution of Working Group I to the Sixth Assessment Report of the Intergovernmental Panel on Climate Change*. Cambridge University Press (In Press).

Cao, Z., Wang, D., Zhang, Z., Zhou, K., Liu, X., Wang, L., et al. (2020). Seasonal dynamics and export of biogenic silica in the upper water column of a large marginal sea, the Northern South China Sea. *Progress in Oceanography*, *188*, 102412. https://doi.org/10.1016/j.pocean.2020.102421

Capelle, D. W., Hawley, A. K., Hallam, S. J., & Tortell, P. D. (2018). A multi-year time-series of N_2O dynamics in a seasonally anoxic fjord: Saanich inlet, British Columbia. *Limnology & Oceanography*, *63*, 524–539. https://doi.org/10.1002/lno.10645

Carrasco, C., Karstensen, J., & Farias, L. (2017). On the nitrous oxide accumulation in intermediate waters of the Eastern South Pacific Ocean. *Frontiers in Marine Science*, *4*, 24. https://doi.org/10.3389/fmars.2017.00024

Charpentier, J., Farias, L., Yoshida, N., Boontanon, N., & Raimbault, P. (2007). Nitrous oxide distribution and its origin in the central and Eastern South Pacific subtropical Gyre. *Biogeosciences*, *4*, 729–741. https://doi.org/10.5194/bg-4-729-2007

Chen, C. C., Shiah, F. K., Chung, S. W., & Liu, K. K. (2006). Winter phytoplankton blooms in the shallow mixed layer of the South China Sea enhanced by upwelling. *Journal of Marine Systems*, *59*, 97–110. https://doi.org/10.1016/j.jmarsys.2005.09.002

Chen, C. T. A., Hou, W. P., Gamo, T., & Wang, S. L. (2006). Carbonate-related parameters of subsurface waters in the West Philippine, South China and Sulu seas. *Marine Chemistry*, *99*, 151–161. https://doi.org/10.1016/j.marchem.2005.05.008

Chen, C. T. A., Wang, S. L., Wang, B. J., & Pai, S. C. (2001). Nutrient budgets for the south China sea basin. *Marine Chemistry*, *75*, 281–300. https://doi.org/10.1016/S0304-4203(01)00041-X

Chen, X. L., Ma, X., Gu, X. J., Liu, S. M., Song, G. D., Jin, H. Y., & Zhang, G. L. (2021). Seasonal and spatial variations of N_2O distribution and emission in the East China Sea and South Yellow sea. *Science of the Total Environment*, *775*, 775. https://doi.org/10.1016/j.scitotenv.2021.145715

Cohen, Y., & Gordon, L. I. (1979). Nitrous oxide production in the ocean. *Journal of Geophysical Research*, *84*, 347–353. https://doi.org/10.1029/JC084iC01p00347

Cornejo, M., Murillo, A. A., & Farias, L. (2015). An unaccounted for N_2O sink in the surface water of the eastern subtropical South Pacific: Physical versus biological mechanisms. *Progress in Oceanography*, *137*, 12–23. https://doi.org/10.1016/j.pocean.2014.12.016

Craig, H., & Gordon, L. I. (1963). Nitrous oxide in the ocean and the marine atmosphere. *Geochimica et Cosmochimica Acta*, *27*, 949–955. https://doi.org/10.1016/0016-7037(63)90104-2

Dai, M., Cao, Z., Guo, X., Zhai, W., Liu, Z., Yin, Z., et al. (2013). Why are some marginal seas sources of atmospheric CO_2? *Geophysical Research Letters*, *40*, 2154–2158. https://doi.org/10.1002/grl.50390

Dai, M., Su, J., Zhao, Y., Hofmann, E. E., Cao, Z., Cai, W.-J., et al. (2022). Carbon fluxes in the coastal ocean: Synthesis, boundary processes and future trends. *Annual Review of Earth and Planetary Sciences*, *50*, 593–626. https://doi.org/10.1146/annurev-earth-032320-090746

dela Paz, M., García-Ibáñez, M. I., Steinfeldt, R., Rios, A. F., & Pérez, F. F. (2017). Ventilation versus biology: What is the controlling mechanism of nitrous oxide distribution in the North Atlantic? *Global Biogeochemical Cycles*, *31*, 745–760. https://doi.org/10.1002/2016gb005507

Deng, W., Wang, S., Wan, X., Zheng, Z., Jiao, N., Kao, S. J., et al. (2021). Potential competition between marine heterotrophic prokaryotes and autotrophic picoplankton for nitrogen substrates. *Limnology & Oceanography*, *66*, 3338–3355. https://doi.org/10.1002/lno.11883

De Wilde, H. P. J., & Helder, W. (1997). Nitrous oxide in the Somali basin: The role of upwelling. *Deep Sea Research II*, *44*, 1319–1340. https://doi.org/10.1016/S0967-0645(97)00011-8

Dlugokencky, E. (2022). Carbon cycle greenhouse gases: Trends in atmospheric nitrous oxide. *NOAA/GML*. http://gml.noaa.gov/ccgg/trends_n2o/

Du, C., Liu, Z., Dai, M., Kao, S. J., Cao, Z., Zhang, Y., et al. (2013). Impact of the Kuroshio intrusion on the nutrient inventory in the upper Northern South China Sea: Iinsights from an isopycnal mixing model. *Biogeosciences*, *10*, 6419–6432. https://doi.org/10.5194/bg-10-6419-2013

Du, C., Liu, Z., Kao, S. J., & Dai, M. (2017). Diapycnal fluxes of nutrients in an oligotrophic oceanic regime: The South China Sea. *Geophysical Research Letters*, *44*, 11510–11511. https://doi.org/10.1002/2017gl074921

England, M. H. (1995). The age of water and ventilation timescales a global ocean model. *Journal of Physical Oceanography*, *25*, 2756–2777. https://doi.org/10.1175/1520-0485(1995)025<2756:taowav>2.0.co;2

Farías, L., Florez-Leiva, L., Besoain, V., Sarthou, G., & Fernández, C. (2015). Dissolved greenhouse gases (nitrous oxide and methane) associated with the naturally iron-fertilized Kerguelen Region (KEOPS 2 cruise) in the Southern Ocean. *Biogeosciences*, *12*, 1925–1940. https://doi.org/10.5194/bg-12-1925-2015

Forster, G., Upstill-Goddard, R. C., Gist, N., Robinson, C., Uher, G., & Woodward, E. M. S. (2009). Nitrous oxide and methane in the Atlantic Ocean between 50°N and 52°S: Latitudinal distribution and sea-to-air flux. *Deep Sea Research II: Topical Studies in Oceanography*, *56*, 964–976. https://doi.org/10.1016/j.dsr2.2008.12.002

Frame, C. H., & Casciotti, K. L. (2010). Biogeochemical controls and isotopic signatures of nitrous oxide production by a marine ammonia-oxidizing bacterium. *Biogeosciences*, *7*, 2695–2709. https://doi.org/10.5194/bg-7-2695-2010

Frame, C. H., Deal, E., Nevison, C. D., & Casciotti, K. L. (2014). N_2O production in the Eastern South Atlantic: Analysis of N_2O stable isotopic and concentration data. *Global Biogeochemical Cycles*, *28*, 1262–1278. https://doi.org/10.1002/2013gb004790

Freing, A., Wallace, D. W. R., & Bange, H. W. (2012). Global oceanic production of nitrous oxide. *Philosophical Transactions of the Royal Society B: Biological Sciences*, *367*, 1245–1255. https://doi.org/10.1098/rstb.2011.0360

Freing, A., Wallace, D. W. R., Tanhua, T., Walter, S., & Bange, H. W. (2009). North Atlantic production of nitrous oxide in the context of changing atmospheric levels. *Global Biogeochemical Cycles*, *23*, GB4015. https://doi.org/10.1029/2009gb003472

Gan, J., Liu, Z., & Hui, C. R. (2016). A three-layer alternating spinning circulation in the South China Sea. *Journal of Physical Oceanography*, *46*, 2309–2315. https://doi.org/10.1175/jpo-d-16-0044.1

Gebbie, G., & Huybers, P. (2012). The mean age of ocean waters inferred from radiocarbon observations: Sensitivity to surface sources and accounting for mixing histories. *Journal of Physical Oceanography*, *42*, 291–305. https://doi.org/10.1175/jpo-d-11-043.1

Goreau, T. J., Kaplan, W. A., Wofsy, S. C., McElroy, M. B., Valois, F. W., & Watson, S. W. (1980). Production of NO_2^- and N_2O by nitrifying bacteria at reduced concentrations of oxygen. *Applied and Environmental Microbiology*, *40*, 526–532. https://doi.org/10.1128/aem.40.3.526-532.1980

Gu, X. J., Cheng, F., Chen, X. L., Du, G. X., & Zhang, G. L. (2021). Dissolved nitrous oxide and hydroxylamine in the South Yellow Sea and the East China Sea during early spring: Distribution, production, and emissions. *Frontiers in Marine Science*, *8*. https://doi.org/10.3389/fmars.2021.725713

Guerrero-Feijóo, E., Sintes, E., Herndl, G. J., & Varela, M. M. (2018). High dark inorganic carbon fixation rates by specific microbial groups in the Atlantic off the Galician Coast (NW Iberian margin). *Environmental Microbiology*, *20*, 602–611. https://doi.org/10.1111/1462-2920.13984

Han, A., Dai, M., Kao, S. J., Gan, J., Li, Q., Wang, L., et al. (2012). Nutrient dynamics and biological consumption in a large continental shelf system under the influence of both a river plume and coastal upwelling. *Limnology & Oceanography*, *57*, 486–502. https://doi.org/10.4319/lo.2012.57.2.0486

Han, Y., Zhang, G. L., Zhao, Y. C., & Liu, S. M. (2013). Distributions and sea-to-air fluxes of nitrous oxide in the coastal and shelf waters of the Northwestern South China Sea. *Estuarine, Coastal and Shelf Science*, *133*, 32–44. https://doi.org/10.1016/j.ecss.2013.08.001

Horrigan, S. G., Carlucci, A. F., & Williams, P. M. (1981). Light inhibition of nitrification in sea-surface films. *Journal of Marine Research*, *39*, 557–565.

Hu, J., Kawamura, H., Hong, H., & Qi, Y. (2000). A review on the currents in the South China Sea: Seasonal circulation, South China Sea warm current and Kuroshio intrusion. *Journal of Oceanography*, *56*, 607–624. https://doi.org/10.1023/A:1011117531252

Huang, T. H., Chen, C. T. A., Tseng, H. C., Lou, J. Y., Wang, S. L., Yang, L., et al. (2017). Riverine carbon fluxes to the south China sea. *Journal of Geophysical Research: Biogeosciences*, *122*, 1239–1259. https://doi.org/10.3389/10.1002/2016jg003701

Huang, Y., Laws, E., Chen, B., & Huang, B. (2019). Stimulation of heterotrophic and autotrophic metabolism in the mixing zone of the Kuroshio current and Northern South China Sea: Implications for export production. *Journal of Geophysical Research: Biogeosciences*, *124*, 2645–2661. https://doi.org/10.1029/2018jg004833

Ji, Q., Buitenhuis, E., Suntharalingam, P., Sarmiento, J. L., & Ward, B. B. (2018). Global nitrous oxide production determined by oxygen sensitivity of nitrification and denitrification. *Global Biogeochemical Cycles*, *32*, 1790–1802. https://doi.org/10.1029/2018gb005887

Ji, Q., & Ward, B. B. (2017). Nitrous oxide production in surface waters of the mid-latitude North Atlantic Ocean. *Journal of Geophysical Research: Oceans*, *122*, 2612–2621. https://doi.org/10.1002/2016jc012467

Kim, T. W., Lee, K., Duce, R., & Liss, P. (2014). Impact of atmospheric nitrogen deposition on phytoplankton productivity in the South China Sea. *Geophysical Research Letters*, *41*, 3156–3162. https://doi.org/10.1002/2014gl059665

Klawonn, I., Bonaglia, S., Bruchert, V., & Ploug, H. (2015). Aerobic and anaerobic nitrogen transformation processes in N_2-fixing cyanobacterial aggregates. *The ISME Journal*, *9*, 1456–1466. https://doi.org/10.1038/ismej.2014.232

Kock, A., Arévalo-Martínez, D. L., Löscher, C. R., & Bange, H. W. (2016). Extreme N_2O accumulation in the coastal oxygen minimum zone off Peru. *Biogeosciences*, *13*, 827–840. https://doi.org/10.5194/bg-13-827-2016

Kock, A., Schafstall, J., Dengler, M., Brandt, P., & Bange, H. W. (2012). Sea-to-air and diapycnal nitrous oxide fluxes in the eastern tropical North Atlantic ocean. *Biogeosciences*, *9*, 957–964. https://doi.org/10.5194/bg-9-957-2012

Kozlowski, J. A., Stieglmeier, M., Schleper, C., Klotz, M. G., & Stein, L. Y. (2016). Pathways and key intermediates required for obligate aerobic ammonia-dependent chemolithotrophy in bacteria and *Thaumarchaeota*. *The ISME Jorunal*, *10*, 1836–1845. https://doi.org/10.1038/ismej.2016.2

Kraft, B., Jehmlich, N., Larsen, M., Bristow, L. A., Könneke, M., Thamdrup, B., & Canfield, D. E. (2022). Oxygen and nitrogen production by an ammonia-oxidizing Archaeon. *Science*, *375*, 97–100. https://doi.org/10.1126/science.abe6733

Landolfi, A., Somes, C. J., Koeve, W., Zamora, L. M., & Oschlies, A. (2017). Oceanic nitrogen cycling and N_2O flux perturbations in the anthropocene. *Global Biogeochemical Cycles*, *31*, 1236–1255. https://doi.org/10.1002/2017GB005633

Law, C. S., & Owens, N. J. P. (1990). Significant flux of atmospheric nitrous oxide from the Northwest Indian Ocean. *Nature*, *346*, 826–828. https://doi.org/10.1038/346826a0

Li, Q., Guo, X., Zhai, W., Xu, Y., & Dai, M. (2020). Partial pressure of CO_2 and air-sea CO_2 fluxes in the South China Sea: Synthesis of an 18-year dataset. *Progress in Oceanography*, *182*, 102272. https://doi.org/10.1016/j.pocean.2020.102272

Li, X., Wu, K., Gu, S., Jiang, P., Li, H., Liu, Z., & Dai, M. (2021). Enhanced biodegradation of dissolved organic carbon in the Western boundary Kuroshio Current when intruded to the marginal South China Sea. *Journal of Geophysical Research: Oceans*, *126*, e2021JC017585. https://doi.org/10.1029/2021jc017585

Li, X. X., Zhang, Z. R., Wade, T. L., Knap, A. H., & Zhang, C. L. L. (2017). Sources and compositional distribution of organic carbon in surface sediments from the lower Pearl River to the coastal South China Sea. *Journal of Geophysical Research: Biogeosciences*, *122*, 2104–2117. https://doi.org/10.1002/2017jg003981

Li Chen, Y. L. (2005). Spatial and seasonal variations of nitrate-based new production and primary production in the South China Sea. *Deep Sea Research Part I: Oceanographic Research Papers*, *52*, 319–340. https://doi.org/10.1016/j.dsr.2004.11.001

Lin, H., Dai, M., Kao, S. J., Wang, L., Roberts, E., Yang, J. Y. T., et al. (2016). Spatiotemporal variability of nitrous Oxide in a large eutrophic estuarine system: The Pearl River Estuary, China. *Marine Chemistry*, *182*, 14–24. https://doi.org/10.1016/j.marchem.2016.03.005

Liu, Z., & Gan, J. (2017). Three-dimensional pathways of water masses in the south China sea: A modeling study. *Journal of Geophysical Research: Oceans*, *122*, 6039–6054. https://doi.org/10.1002/2016JC012511

Lu, Z., Gan, J., Dai, M., Zhao, X., & Hui, C. R. (2020). Nutrient transport and dynamics in the south China sea: A modeling study. *Progress in Oceanography*, *183*, 102308. https://doi.org/10.1016/j.pocean.2020.102308

Ma, X., Lennartz, S. T., & Bange, H. W. (2019). A multi-year observation of nitrous oxide at the Boknis Eck time series station in the Eckernförde Bay (southwestern Baltic sea). *Biogeosciences*, *16*, 4097–4111. doi : https://doi.org/10.5194/bg-16-4097-2019

MacFarling Meure, C., Etheridge, D., Trudinger, C., Steele, P., Langenfelds, R., van Ommen, T., et al. (2006). Law Dome CO_2, CH_4 and N_2O ice core records extended to 2000 years BP. *Geophysical Research Letters*, *33*(14), L14810. https://doi.org/10.1029/2006gl026152

Manizza, M., Keeling, R. F., & Nevison, C. D. (2012). On the processes controlling the seasonal cycles of the Air-sea fluxes of O_2 and N_2O: A modelling study. *Tellus B: Chemical and Physical Meteorology*, *64*, 18429. https://doi.org/10.3402/tellusb.v64i0.18429

Martinez-Rey, J., Bopp, L., Gehlen, M., Tagliabue, A., & Gruber, N. (2015). Projections of oceanic N_2O emissions in the 21st century using the IPSL Earth system model. *Biogeosciences*, *12*, 4133–4148. https://doi.org/10.5194/bg-12-4133-2015

Marty, D., Bonin, P., Michotey, V., & Bianchi, M. (2001). Bacterial biogas production in coastal systems affected by freshwater inputs. *Continental Shelf Research*, *21*, 2105–2115. https://doi.org/10.1016/S0278-4343(01)00045-0

Murray, R. H., Erler, D. V., & Eyre, B. D. (2015). Nitrous oxide fluxes in estuarine environments: Response to global change. *Global Change Biology*, *21*, 3219–3245. https://doi.org/10.1111/gcb.12923

Naqvi, S. W. A., Bange, H. W., Farías, L., Monteiro, P. M. S., Scranton, M. I., & Zhang, J. (2010). Marine hypoxia/anoxia as a source of CH_4 and N_2O. *Biogeosciences*, *7*, 2159–2190. https://doi.org/10.5194/bg-7-2159-2010

Nevison, C., Butler, J. H., & Elkins, J. W. (2003). Global distribution of N_2O and the ΔN_2O-AOU yield in the subsurface ocean. *Global Biogeochemical Cycles*, *17*, 119. https://doi.org/10.1029/2003GB002068

Nevison, C. D., Keeling, R. F., Weiss, R. F., Popp, B. N., Jin, X., Fraser, P. J., et al. (2005). Southern Ocean ventilation inferred from seasonal cycles of atmospheric N_2O and O_2/N_2 at Cape Grim, Tasmania. *Tellus B: Chemical and Physical Meteorology*, *57*, 218–229. https://doi.org/10.1111/j.1600-0889.2005.00143.x

Nevison, C. D., Weiss, R. F., & Erickson, D. J. (1995). Global oceanic emissions of nitrous oxide. *Journal of Geophysical Research*, *100*, 15809–15820. https://doi.org/10.1029/95JC00684

Ning, X., Chai, F., Xue, H., Cai, Y., Liu, C., & Shi, J. (2004). Physical-biological oceanographic coupling influencing phytoplankton and primary production in the South China Sea. *Journal of Geophysical Research*, *109*, C10005. https://doi.org/10.1029/2004jc002365

Olson, R. J. (1981). Differential photoinhibition of marine nitrifying bacteria: A possible mechanism for the formation of the primary nitrite maximum. *Journal of Marine Research*, *39*, 227–238.

Ostrom, N. E., Russ, M. E., Popp, B., Rust, T. M., & Karl, D. M. (2000). Mechanisms of nitrous oxide production in the Subtropical North Pacific based on determinations of the isotopic abundances of nitrous oxide and di-oxygen. *Chemosphere - Global Change Science*, *2*, 281–290. https://doi.org/10.1016/S1465-9972(00)00031-3

Pachiadaki, M. G., Sintes, E., Bergauer, K., Brown, J. M., Record, N. R., Swan, B. K., et al. (2017). Major role of nitrite-oxidizing bacteria in dark ocean carbon fixation. *Science*, *358*, 1046–1051. https://doi.org/10.1126/science.aan8260

Popp, B. N., Westley, M. B., Toyoda, S., Miwa, T., Dore, J. E., Yoshida, N., et al. (2002). Nitrogen and oxygen isotopomeric constraints on the origins and sea-to-air flux of N_2O in the pligotrophic Subtropical North Pacific Gyre. *Global Biogeochemical Cycles*, *16*, 1064. https://doi.org/10.1029/2001GB001806

Prinn, R. G., Weiss, R. F., Arduini, J., Arnold, T., DeWitt, H. L., Fraser, P. J., et al. (2018). History of chemically and radiatively important atmospheric gases from the advanced global atmospheric gases experiment (AGAGE). *Earth System Science Data*, *10*, 985–1018. https://doi.org/10.5194/essd-10-985-2018

Qin, W., Meinhardt, K. A., Moffett, J. W., Devol, A. H., Virginia Armbrust, E., Ingalls, A. E., & Stahl, D. A. (2017). Influence of oxygen availability on the activities of ammonia-oxidizing archaea. *Environmental Microbiology Report*, *3*, 250–256. https://doi.org/10.1111/1758-2229.12525

Ravishankara, A. R., Daniel, J. S., & Portmann, R. W. (2009). Nitrous oxide (N_2O): The dominant ozone-depleting substance emitted in the 21st century. *Science*, *326*, 123–125. https://doi.org/10.1126/science.1176985

Rees, A. P., Brown, I. J., Jayakumar, A., & Ward, B. B. (2016). The inhibition of N_2O production by ocean acidification in cold temperate and polar waters. *Deep Sea Research Part II: Topical Studies in Oceanography*, *127*, 93–101. https://doi.org/10.1016/j.dsr2.2015.12.006

Shiozaki, T., Ijichi, M., Isobe, K., Hashihama, F., Nakamura, K., Ehama, M., et al. (2016). Nitrification and its influence on biogeochemical cycles from the equatorial Pacific to the Arctic Ocean. *The ISME Journal*, *10*, 2184–2197. https://doi.org/10.1038/ismej.2016.18

Stein, L. Y., & Yung, Y. L. (2003). Production, isotopic composition, and atmospheric fate of biologically produced nitrous oxide. *Annual Review of Earth and Planetary Sciences*, *31*, 329–356. https://doi.org/10.1146/annurev.earth.31.110502.080901

Stief, P., Kamp, A., Thamdrup, B., & Glud, R. N. (2016). Anaerobic nitrogen turnover by sinking diatom aggregates at varying ambient oxygen levels. *Frontiers in Microbiology*, *7*, 98. https://doi.org/10.3389/fmicb.2016.00098

Stieglmeier, M., Mooshammer, M., Kitzler, B., Wanek, W., Zechmeister-Boltenstern, S., Richter, A., & Schleper, C. (2014). Aerobic nitrous oxide production through N-nitrosating hybrid formation in ammonia-oxidizing archaea. *The ISME Journal*, *8*, 1135–1146. https://doi.org/10.1038/ismej.2013.220

Sun, X., Jayakumar, A., Tracey, J. C., Wallace, E., Kelly, C. L., Casciotti, K. L., & Ward, B. B. (2020). Microbial N_2O consumption in and above marine N_2O production hotspots. *The ISME Journal*, *15*, 1434–1444. https://doi.org/10.1038/s41396-020-00861-2

Sun, X., Jayakumar, A., & Ward, B. B. (2017). Community composition of nitrous oxide consuming bacteria in the oxygen minimum zone of the Eastern Tropical South Pacific. *Frontiers in Microbiology*, *8*, 1183. https://doi.org/10.3389/fmicb.2017.01183

Suntharalingam, P., Buitenhuis, E., Le Quéré, C., Dentener, F., Nevison, C., Butler, J. H., et al. (2012). Quantifying the impact of anthropogenic nitrogen deposition on oceanic nitrous oxide. *Geophysical Research Letters*, *39*, L07605. https://doi.org/10.1029/2011GL050778

Suntharalingam, P., Zamora, L. M., Bange, H. W., Bikkina, S., Buitenhuis, E., Kanakidou, M., et al. (2019). Anthropogenic nitrogen inputs and impacts on oceanic N_2O fluxes in the Northern Indian Ocean: The need for an integrated observation and modelling approach. *Deep-Sea Research II*, *166*, 104–113. https://doi.org/10.1016/j.dsr2.2019.03.007

Tian, H., Xu, R., Canadell, J. G., Thompson, R. L., Winiwarter, W., Suntharalingam, P., et al. (2020). A comprehensive quantification of global nitrous oxide sources and sinks. *Nature*, *586*, 248–256. https://doi.org/10.1038/s41586-020-2780-0

Trottet, A., Leboulanger, C., Vidussi, F., Pete, R., Bouvy, M., & Fouilland, E. (2016). Heterotrophic bacteria show weak com- petition for nitrogen in Mediterranean coastal waters (Thau Lagoon) in autumn. *Microbial Ecology*, *71*, 304–314. https://doi.org/10.1007/s00248-015-0658-8

Tseng, C. M., Wong, G. T. F., Lin, I. I., Wu, C. R., & Liu, K. K. (2005). A unique seasonal pattern in phytoplankton biomass in low-latitude waters in the South China Sea. *Geophysical Research Letters*, *32*, L08608. https://doi.org/10.1029/2004gl022111

Tseng, H. C., Chen, C. T. A., Borges, A. V., DelValls, T. A., Lai, C. M., & Chen, T. Y. (2016). Distributions and sea-to-air fluxes of nitrous oxide in the south China Sea and the west Philippines sea. *Deep-Sea Research I*, *115*, 131–144. https://doi.org/10.1016/j.dsr.2016.06.006

Walter, S., Bange, H. W., Breitenbach, U., & Wallace, D. W. R. (2006). Nitrous oxide in the north Atlantic ocean. *Biogeosciences*, *4*, 607–619. https://doi.org/10.5194/bg-3-607-2006

Wan, X. S., Sheng, H. X., Dai, M., Zhang, Y., Shi, D., Trull, T. W., et al. (2018). Ambient nitrate switches the ammonium consumption pathway in the euphotic ocean. *Nature Communication*, *9*, 915. https://doi.org/10.1038/s41467-018-03363-0

Wanninkhof, R. (2014). Relationship between wind speed and gas exchange over the ocean revisited. *Limnology and Oceanography: Methods*, *12*, 351–362. https://doi.org/10.4319/lom.2014.12.351

Wanninkhof, R., Asher, W. E., Ho, D. T., Sweeney, C., & McGillis, W. R. (2009). Advances in quantifying air-sea gas exchange and environmental forcing. *Annual Review of Marine Science*, *1*, 213–244. https://doi.org/10.1146/annurev.marine.010908.163742

Weiss, R. F., & Price, B. A. (1980). Nitrous oxide solubility in water and seawater. *Marine Chemistry*, *8*, 347–359. https://doi.org/10.1016/0304-4203(80)90024-9

Westley, M. B., Yamagishi, H., Popp, B. N., & Yoshida, N. (2006). Nitrous oxide cycling in the Black Sea inferred from stable isotope and isotopomer distributions. *Deep-Sea Research II*, *53*, 1802–1816. https://doi.org/10.1016/j.dsr2.2006.03.012

Wilson, S. T., Al-Haj, A. N., Bourbonnais, A., Frey, C., Fulweiler, R. W., Kessler, J. D., et al. (2020). Ideas and perspectives: A strategic assessment of methane and nitrous oxide measurements in the marine environment. *Biogeosciences*, *17*, 5809–5828. https://doi.org/10.5194/bg-17-5809-2020

Wilson, S. T., Ferrón, S., & Karl, D. M. (2017). Interannual variability of methane and nitrous oxide in the North Pacific Subtropical Gyre. *Geophysical Research Letters*, *44*, 9885–9892. https://doi.org/10.1002/2017gl074458

Wong, G. T. F., Ku, T. L., Mulholland, M., Tseng, C. M., & Wang, D. P. (2007). The SouthEast Asian time-series study (SEATS) and the biogeochemistry of the south China sea—an overview. *Deep-Sea Research II*, *54*, 1434–1447. https://doi.org/10.1016/j.dsr2.2007.05.012

Wrage, N., Velthof, G. L., van Beusichem, M. L., & Oenema, O. (2001). Role of nitrifier denitrification in the production of nitrous oxide. *Soil Biology and Biochemistry*, *33*, 1723–1732. https://doi.org/10.1016/s0038-0717(01)00096-7

Wu, J., Lao, Q., Chen, F., Huang, C., Zhang, S., Wang, C., et al. (2021). Water mass processes between the south China Sea and the Western Pacific through the Luzon Strait: Insights from hydrogen and oxygen isotopes. *Journal of Geophysical Research: Oceans*, *126*, e2021JC017484. https://doi.org/10.1029/2021jc017484

Wyman, M., Hodgson, S., & Bird, C. (2013). Denitrifying Alphaproteobacteria from the Arabian Sea that express nosZ, the gene encoding nitrous oxide reductase, in oxic and suboxic waters. *Applied and Environmental Microbiology*, *79*, 2670–2681. https://doi.org/10.1128/aem.03705-12

Xu, M. N., Zhang, W., Zhu, Y., Liu, L., Zheng, Z., Wan, X. S., et al. (2018). Enhanced ammonia oxidation caused by lateral Kuroshio intrusion in the boundary zone of the Northern South China Sea. *Geophysical Research Letters*, *45*, 6585–6593. https://doi.org/10.1029/2018gl077896

Yang, S., Chang, B. X., Warner, M. J., Weber, T. S., Bourbonnais, A. M., Santoro, A. E., et al. (2020). Global reconstruction reduces the uncertainty of oceanic nitrous oxide emissions and reveals a vigorous seasonal cycle. *Proceedings of the National Academy of Sciences*, *117*, 11954–11960. https://doi.org/10.1073/pnas.1921914117

Yoshida, N., Morimoto, H., Hirano, M., Koike, I., Matsuo, S., Wada, E., et al. (1989). Nitrification rates and ^{15}N abundances of N_2O and NO_3^- in the Western North Pacific. *Nature*, *342*, 895–897. https://doi.org/10.1038/342895a0

Yoshinari, T. (1976). Nitrous oxide in the sea. *Marine Chemistry*, *4*, 189–202. https://doi.org/10.1016/0304-4203(76)90007-4

Zhai, W. D., Dai, M. H., Chen, B. S., Guo, X. H., Li, Q., Shang, S. L., et al. (2013). Seasonal variations of sea–air CO_2 fluxes in the largest tropical marginal sea (South China Sea) based on multiple-year underway measurements. *Biogeosciences*, *10*, 7775–7791. https://doi.org/10.5194/bg-10-7775-2013

Zhang, G. L., Liu, S. M., Casciotti, K. L., Forbes, M. S., Gu, X. J., Ren, Y. Y., & Zheng, W. J. (2019). Distribution of concentration and stable isotopic composition of N_2O in the shelf and slope of the Northern South China Sea: Implications for production and emission. *Journal of Geophysical Research: Oceans*, *124*, 6218–6234. https://doi.org/10.1029/2019jc014947

Zhang, H., & Li, S. Y. (2000). Effects of physical and biochemical processes on the dissolved oxygen budget for the Pearl River Estuary during summer. *Journal of Marine Systems*, *79*, 65–88. https://doi.org/10.1016/j.jmarsys.2009.07.002

Zhang, Y., Qin, W., Hou, L., Zakem, E. J., Wan, X., Zhao, Z., et al. (2020). Nitrifier aadaptation to low energy flux controls inventory of reduced nitrogen in the dark ocean. *Proceedings of the National Academy of Sciences*, *117*, 4823–4830. https://doi.org/10.1073/pnas.1912367117

Zhu, Y., Liu, J., Mulholland, M. R., Du, C., Wang, L., Widner, B., et al. (2021). Dynamics of ammonium biogeochemistry in an oligotrophic regime in the South China Sea. *Marine Chemistry*, *237*, 104040. https://doi.org/10.1016/j.marchem.2021.104040

Zhu, Y., Sun, J., Wang, Y., Li, S., Xu, T., Wei, Z., & Qu, T. (2019). Overview of the multi-layer circulation in the south China sea. *Progress in Oceanography*, *175*, 171–182. https://doi.org/10.1016/j.pocean.2019.04.001